

On the Plutinos and Twotinos of the Kuiper Belt

E. I. Chiang & A. B. Jordan

*Center for Integrative Planetary Sciences
Astronomy Department
University of California at Berkeley
Berkeley, CA 94720, USA*

echiang@astron.berkeley.edu, abjordan@uclink.berkeley.edu

ABSTRACT

We illuminate dynamical properties of Kuiper Belt Objects (KBOs) in the 3:2 (“Plutino”) and 2:1 (“Twotino”) Neptunian resonances within the model of resonant capture and migration. We analyze a series of numerical integrations, each involving the 4 migratory giant planets and 400 test particles distributed throughout trans-Neptunian space, to measure the efficiencies of capture into the 3:2 and 2:1 resonances, the efficiencies of capture into Kozai-type secular resonances, and the libration centers and amplitudes of resonant particles, all as functions of the migration speed. We synthesize instantaneous snapshots of the spatial distribution of $\sim 10^4$ resonant KBOs, from which we derive the longitudinal variation of the sky density of each resonant family. Twotinos cluster $\pm 75^\circ$ away from Neptune’s longitude, while Plutinos cluster $\pm 90^\circ$ away. Such longitudinal clustering persists even for surveys that are not volume-limited in their ability to detect resonant KBOs. Remarkably, between -90° and -60° of Neptune’s longitude, we find the ratio of sky densities of Twotinos to Plutinos to be nearly unity despite the greater average distance of Twotinos, assuming the two resonant populations are equal in number and share the same size, albedo, and inclination distributions. We couple our findings to observations to crudely estimate that the intrinsic Twotino population is within a factor of ~ 3 of the Plutino population. Most strikingly, the migration model predicts a possible asymmetry in the spatial distribution of Twotinos: more Twotinos may lie at longitudes behind that of Neptune than ahead of it. The magnitude of the asymmetry amplifies dramatically with faster rates of migration and can be as large as $\sim 300\%$. A differential measurement of the sky density of 2:1 resonant objects behind of and in front of Neptune’s longitude would powerfully constrain the migration history of that planet.

Subject headings: Kuiper Belt — comets: general — minor planets, asteroids — celestial mechanics

1. INTRODUCTION

The substantial eccentricity, e_p , of Pluto’s orbit is well explained by Malhotra’s (1995) theory of resonant capture by Neptune. In this scenario, Neptune migrated radially outwards from the sun by scattering planetesimals towards Jupiter, captured Pluto into its 3:2 mean-motion resonance, and amplified e_p upon continuing its migration. The resonant amplification of e_p can be understood either mechanistically using Gauss’s equations (see, e.g., Peale 1986), or in terms of the preservation of an adiabatic invariant (see, e.g., Yu & Tremaine 2001). The discovery of dozens of Kuiper Belt Objects (KBOs) that share the 3:2 Neptunian resonance with Pluto and that also exhibit large orbital eccentricities (Jewitt & Luu 2000) apparently vindicates this proposal that Neptune plowed its way outwards through a field of planetesimals early in the history of the solar system (Fernandez & Ip 1984).

In the particular numerical simulation presented by Malhotra (1995), the 2:1 Neptunian resonance is predicted to be about as equally populated as the 3:2 resonance. For brevity, we will refer to KBOs in the latter resonance as “Plutinos” and KBOs in the former resonance as “Twotinos.” As of July 4, 2002, the Minor Planet Center (MPC) database contains ~ 41 Plutino candidates (objects observed at multiple oppositions having fitted semi-major axes, a , within 0.3 AU of the exact 3:2 resonance location at $a_{3:2} = 39.5$ AU), and ~ 5 Twotino candidates (objects whose a ’s lie within 0.3 AU of the exact 2:1 resonance location at $a_{2:1} = 47.8$ AU).¹ The Twotino candidates possess substantial orbital eccentricities, $e \approx 0.2$ – 0.4 , in accord with the predictions of resonant capture and migration. Membership in a resonance is confirmed by verifying that the appropriate resonant argument librates rather than circulates (see §2); an orbit classification scheme based on this more rigorous criterion is currently being developed by the Deep Ecliptic Survey (DES) Team (see Millis et al. 2002). For the present paper, we will consider the *observed* Twotinos to be outnumbered by the *observed* Plutinos by a factor of $F_{obs} \sim 8$. Part of this bias must simply reflect the fact that $a_{2:1} > a_{3:2}$; all other factors being equal, more distant objects are fainter and more difficult to detect. But part of this bias may also reflect selection effects that depend on the longitude

¹<http://cfa-www.harvard.edu/iau/lists/TNOs.html>

and latitude of observation. A mean-motion resonant object will be preferentially found at certain locations with respect to Neptune—what we will call “sweet spots” on the sky. The sweet spots for Twotinos are not necessarily those of Plutinos.

Ida et al. (2000) point out that Neptune’s ability to resonantly capture objects varies with migration timescale. A migration timescale that is 20 times shorter than that considered by Malhotra (1995) is found to severely reduce the probability of capture into the 2:1 resonance. For the 3:2 resonance, the capture probability is affected less dramatically by reductions in the migration timescale. The relative robustness of the 3:2 resonance compared to the 2:1 resonance is explored analytically by Friedland (2001), who underscores the importance of the indirect potential for the latter resonance.

This paper quantifies, within the confines of the model of resonant migration, the bias against finding KBOs in the 2:1 resonance over those in the 3:2 resonance. In §2, we set forth general, model-independent considerations for calculating this bias. In §3, we describe in detail the results of a particular simulation of resonant migration. In this section, we present illustrative snapshots of the instantaneous spatial distributions of Twotinos and of Plutinos. In §4, we explore how our results change by varying the migration rate of Neptune. In §5, we discuss our theoretical results in the context of the observations. There, we begin to examine critically the belief that Plutinos intrinsically outnumber Twotinos. A summary of our main findings is provided in §6. Our computations may serve not only to de-bias extant observations and thereby constrain the true relative resonant populations, but also to guide future observational surveys.

2. GENERAL CONSIDERATIONS

The ability of an observational survey to detect KBOs residing within a given resonance depends on the KBOs’ (1) spatial distribution, and (2) size and albedo distributions. In this section, we offer comments regarding the former consideration.

2.1. Mean-Motion Resonances

By definition, an object inhabits a $j+1:j$ outer Neptunian resonance if the resonant argument,

$$\Phi_{j+1:j} \equiv (j+1)\lambda - j\lambda_N - \tilde{\omega}, \quad (1)$$

librates (undergoes a bounded oscillation about a particular angle). Here j is a positive integer, λ and $\tilde{\omega}$ are the mean longitude and longitude of periastron of the object, respectively, and λ_N is the mean longitude of Neptune. A restricted range for $\Phi_{j+1:j}$ implies that the resonant particle will most likely be found at particular longitudes with respect to Neptune. For example, if an object inhabits the $j = 1$ resonance such that $\Phi_{2:1}$ librates about 180° with a negligibly small libration amplitude, then such an object attains perihelion when Neptune is 180° away in longitude. The eccentricity of the resonant object may be so large that the orbits of Neptune and of the particle cross, but the particle avoids close encounters with Neptune by virtue of the boundedness of $\Phi_{2:1}$.

It has been remarked that because $\Phi_{3:2}$ for Pluto and the Plutinos librates about a mean value of $\langle\Phi_{3:2}\rangle = 180^\circ$, these objects tend to be found at longitudes displaced $\pm 90^\circ$ from Neptune when they reach perihelion and are at their brightest (e.g., Jewitt, Luu, & Trujillo 1998). This argument is not strictly correct; it neglects the Plutinos’ often substantial libration amplitudes, $\Delta\Phi_{3:2}$. Just as a librating pendulum is most likely found near the turning points of its trajectory, a Plutino’s resonant argument is most likely found near $\langle\Phi_{3:2}\rangle + \Delta\Phi_{3:2}$ or near $\langle\Phi_{3:2}\rangle - \Delta\Phi_{3:2}$, not $\langle\Phi_{3:2}\rangle$. Figures 1a and 1b portray two toy models for the spatial distributions of 3:2 resonant objects. They demonstrate that the spatial distribution of resonant particles is sensitive to the distribution of libration amplitudes, $dN/d\Delta\Phi$, and not just to the value of the libration center, $\langle\Phi\rangle$. For each panel, the instantaneous locations of 15000 co-planar particles are calculated according to the following scheme: semi-major axes are randomly chosen from a uniform distribution between 39.0 and 39.8 AU, mean longitudes are randomly drawn from a uniform distribution between 0° and 360° , and eccentricities are randomly selected from a uniform distribution between 0.1 and 0.3. Resonant arguments of particles are taken to equal $\Phi_{3:2} = \pm 180^\circ + \Delta\Phi_{3:2} \sin A$, where the upper and lower signs are equally probable and A is randomly drawn from a uniform distribution between 0° and 360° . For Figure 1a, $\Delta\Phi_{3:2}$ is randomly selected from a uniform distribution between 100° and 120° , and for Figure 1b, the underlying distribution for $\Delta\Phi_{3:2}$ is given by the solid histogram in Figure 6. The longitude of perihelion of each particle is calculated according to $\tilde{\omega} = 3\lambda - 2\lambda_N - \Phi_{3:2}$, where λ_N is assigned its present-day value of 302° .

The resultant plots illustrate two ways that Plutinos could be distributed, both of which are possible in principle. In Figure 1a, the objects cluster in 4 locations, respecting the 2×2 turning points of the resonant argument—2 turning points for each of the 2 libration centers, $\langle\Phi_{3:2}\rangle = \pm 180^\circ$. Thus, it is not true *a priori* that 3:2 resonant objects must cluster at only two locations in the sky. By contrast, in Figure 1b, there are enough small-amplitude librators ($\Delta\Phi_{3:2} < 1$ rad) that the concentration of objects does gently peak at longitudes $\pm 90^\circ$ away from Neptune, in abeyance with the usual expectation.

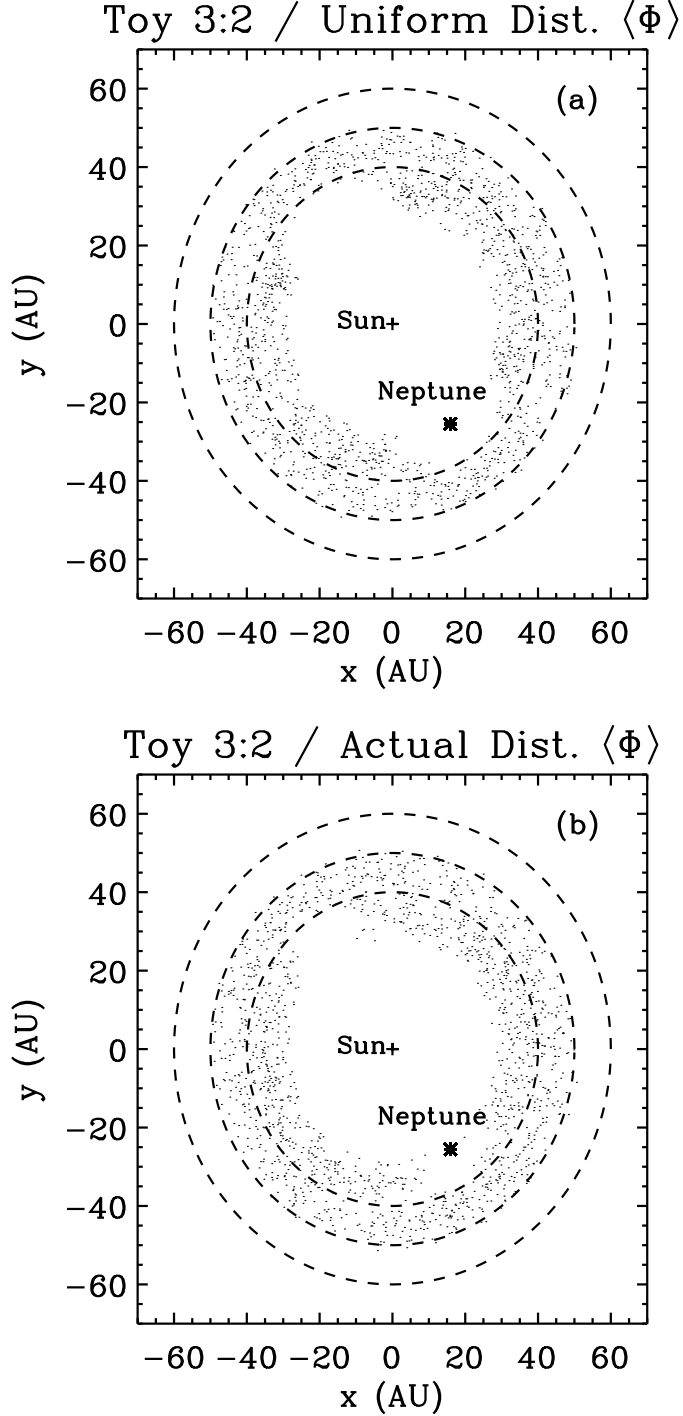


Fig. 1.— Toy models for the spatial distribution of Plutinos. The particles’ resonant arguments equal $\Phi_{3:2} = \pm 180^\circ + \Delta\Phi_{3:2} \sin A$, where A is uniformly distributed between 0° and 360° . In panel (a), $\Delta\Phi_{3:2}$ is uniformly distributed between 100° and 120° . In panel (b), $\Delta\Phi_{3:2}$ reflects the distribution obtained through simulation Ia, as shown by the solid histogram of Figure 6. Where Plutinos cluster depends sensitively on the distribution of $\Delta\Phi_{3:2}$. The dashed circles delimit radii of 40, 50, and 60 AU.

Toy models such as these are useful for analyzing the results of numerical orbit integrations. In anticipation of such integrations, we present Figure 2, which displays a toy model for the distribution of Twotinos. The parameters of the model are described in the figure caption.

2.2. Secular Resonances

Secular resonances might also play a role in determining the spatial distribution of KBOs. Chief among these are Kozai-type resonances in which ω , the argument of perihelion, librates about particular angles, usually $\pm 90^\circ$, 0° , or 180° . Pluto inhabits a Kozai resonance established by the total secular potential of all 4 giant planets, such that its ω librates about 90° with an amplitude of 23° (for a review, see Malhotra & Williams 1997). Thus, Pluto attains perihelion and is brightest only when it sits above the invariable plane by its orbital inclination of $i_p \approx 16^\circ$. If enough Plutinos inhabit Pluto-like Kozai resonances, their detection would be influenced by selection effects that depend on the latitude of observation.

How many Plutinos and Twotinos inhabit Kozai-type resonances? Nesvorný, Roig, & Ferraz-Mello (2000) find that few observed Plutinos, ~ 2 – 4 out of 33, exhibit libration of ω . They explore a scenario by which Pluto gravitationally scatters other Plutinos out of the Kozai resonance. They find the scenario to be viable, though whether it is required by the model of resonant capture and migration is unknown; the efficiency of capture into a Pluto-like Kozai resonance in Malhotra’s (1995) model of planetary migration might already be small enough to explain the observations. Unlike the case for the 3:2 resonance, we are not aware of any study of the possibility of ω -libration within the 2:1 resonance. In §3.4 below, we investigate by direct numerical simulation the capture probability into Kozai-type resonances for both Plutinos and Twotinos within the model of planetary migration.

3. MIGRATION MODEL

Here we describe our model for the radial migration of the four giant planets and the resonant capture of planetesimals. Model ingredients are supplied in §3.1, mean-motion resonance capture efficiencies are computed in §3.2, mean-motion resonance libration statistics and retainment efficiencies are discussed in §3.3, and the statistics of secular resonance capture are presented in §3.4. Those readers interested in the spatial distribution of resonant objects may skip to §3.5 without much loss of continuity.

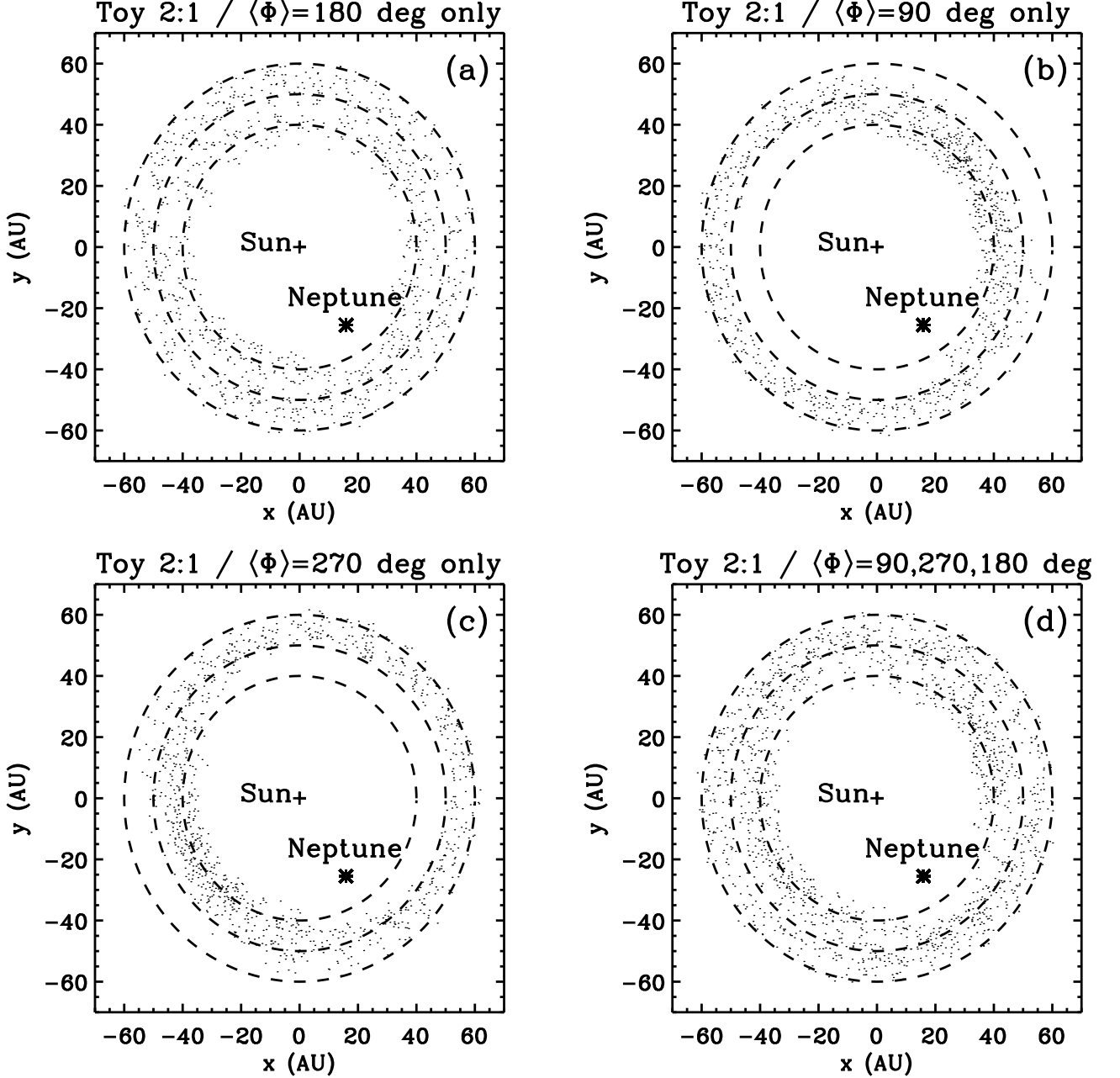


Fig. 2.— Toy models for the spatial distribution of Twotinos. Each panel portrays particles having libration centers, $\langle\Phi_{2:1}\rangle$, that are indicated by the panel title. For $\langle\Phi_{2:1}\rangle = 180^\circ$, particles avoid Neptune’s longitude and are distributed symmetrically about the Sun-Neptune line. For $\langle\Phi_{2:1}\rangle = 90^\circ$ (270°), particles cluster 90° ahead (behind) of Neptune’s longitude. The combination of these libration centers in the proportions found in simulation Ib yields panel (d), which resembles Figure 15. Toy model parameters are uniformly distributed over the following ranges: $47.2\text{ AU} \leq a \leq 48.4\text{ AU}$, $0.1 \leq e \leq 0.3$, $0^\circ \leq \lambda < 360^\circ$, $0^\circ \leq A < 360^\circ$, $135^\circ \leq \Delta\Phi_{2:1} \leq 150^\circ$ if $\langle\Phi_{2:1}\rangle = 180^\circ$, and $15^\circ \leq \Delta\Phi_{2:1} \leq 60^\circ$ otherwise.

3.1. Initial Conditions and Migration Prescription

To effect the migration, we follow Malhotra (1995) and introduce a perturbative acceleration on each planet of the form

$$\delta\ddot{\mathbf{r}} = -\frac{\hat{v}}{\tau} \left(\sqrt{\frac{GM_\odot}{a_f}} - \sqrt{\frac{GM_\odot}{a_i}} \right) \exp(-t/\tau), \quad (2)$$

where a_i and a_f are the initial and final semi-major axes of a given planet, respectively, G is the gravitational constant, t measures time, τ is a time constant, and \hat{v} is the unit vector pointing in the instantaneous direction of the planet’s velocity. Equation (2) corrects a typographical sign error in equation (7) of Malhotra (1995). This prescription causes each planet’s semi-major axis to evolve according to

$$a(t) = a_f - (a_f - a_i) \exp(-t/\tau), \quad (3)$$

but does not directly induce long-term changes in the planet’s eccentricity and inclination. We adopt values for (a_i, a_f) for each of the planets as follows (in AUs): Jupiter (5.00, 5.20), Saturn (8.78, 9.58), Uranus (16.2, 19.2), and Neptune (23.1, 30.1).

We work in a coordinate system that takes the reference plane to be the invariable plane of the solar system. The positions and velocities of each planet at $t = 0$ are adapted from Cohen, Hubbard, and Oesterwinter (1973), with the positions multiplied by a_i/a_f and the velocities multiplied by $\sqrt{a_f/a_i}$. We employ the symplectic integrator, SyMBA, developed by Duncan, Levison, & Lee (1998), which is based on the algorithm by Wisdom & Holman (1991). The integrator was kindly supplied to us by E. Thommes, M. Duncan, & H. Levison.

For simulations Ia and Ib that are described in §3, we take $\tau = 10^7$ yr. Shorter migration periods of $\tau = 10^6$ yr and $\tau = 10^5$ yr are considered in §4.

In simulation Ia, we focus on the efficiency of capture into, and the resultant dynamics within, the 3:2 resonance. We introduce 400 massless test particles whose initial semi-major axes lie between 31.4 AU (= 1 AU greater than the initial location of the 3:2 resonance) and 38.5 AU (= 1 AU short of the final location of the 3:2 resonance). All particles in this region have the potential to be captured into the sweeping 3:2 resonance. Their initial eccentricities and inclinations are randomly drawn from uniform distributions between 0 and 0.05, and between 0° and $1.4^\circ = 0.025$ rad, respectively. Arguments of periastron (ω), longitudes of ascending nodes (Ω), and mean anomalies (M) are uniformly sampled between 0 and 2π . The duration of the integration spans $t_f^{\text{Ia}} = 6 \times 10^7$ yr = 6τ .

In simulation Ib, we concentrate on the 2:1 resonance. The only essential difference between simulations Ia and Ib is that for the latter, the 400 test particles are distributed initially between 37.7 AU (= 1 AU greater than the initial location of the 2:1 resonance) and 46.8 AU (= 1 AU less than the final location of the 2:1 resonance). Thus, all such particles are potentially captured into the 2:1 resonance. The duration of this simulation is $t_f^{\text{Ib}} = 8 \times 10^7 \text{ yr} = 8\tau$.

3.2. Capture Efficiencies

Of the 400 test particles in simulation Ia, 92 are captured into the 3:2 resonance. By definition, $\Phi_{3:2}$ librates for these 92 objects but circulates for the remaining 308. This capture efficiency of $f_{3:2} \approx 23\%$ reflects (1) the probability of capture into the isolated 3:2 resonant potential just prior to resonance encounter (Henrard & Lemaître 1983, Borderies & Goldreich 1984), (2) losses due to pre-emptive capture into “competing” resonances such as the 5:3 and 2:1 which lie exterior to the 3:2, and (3) losses due to violent scattering by close encounters with the planets. Figure 3 displays the final eccentricities and inclinations versus the semi-major axes of those test particles having $a \leq 60$ AU.

From simulation Ib, we estimate the capture efficiency of the 2:1 resonance to be $f_{2:1} \approx 212/400 = 53\%$. This value is more than twice as high as $f_{3:2}$, reflecting both the lack of competition from other sweeping resonances which lie interior to the 2:1, and the lower probability of scattering by Neptune at these greater distances. Figure 4 displays the final (a, e, i) for those test particles having $a \leq 60$ AU at the close of simulation Ib. Note that many objects remain uncaptured by any low-order resonance at semi-major axes $43 \text{ AU} \lesssim a \lesssim 47 \text{ AU}$; these non-resonant bodies presumably represent members of the low-inclination Classical Kuiper Belt that is observed today (Levison & Stern 2001; Brown 2001).

These capture efficiencies are recorded in Table 1. We emphasize that f represents only the efficiency of capture, as distinct from the efficiency of retainment of captured objects, g , over the age of the solar system. Whether a captured KBO remains in a given resonance over 4×10^9 yr is discussed in §3.3.

Mean inclinations, $\langle i \rangle$, of Plutinos and Twotinos are plotted against mean eccentricities, $\langle e \rangle$, in Figure 5. The mean is taken over the last 1×10^7 yr in simulation Ia, and the last 3×10^7 yr in Ib, during which times the migration has effectively stopped. There is a tendency for the Plutinos to have their $\langle i \rangle$'s and $\langle e \rangle$'s inversely correlated. No apparent correlation exists between $\langle i \rangle$ and $\langle e \rangle$ for the Twotinos. The predicted inclinations seem too low to compare favorably with the observed inclinations; the inadequacy of the migration model in

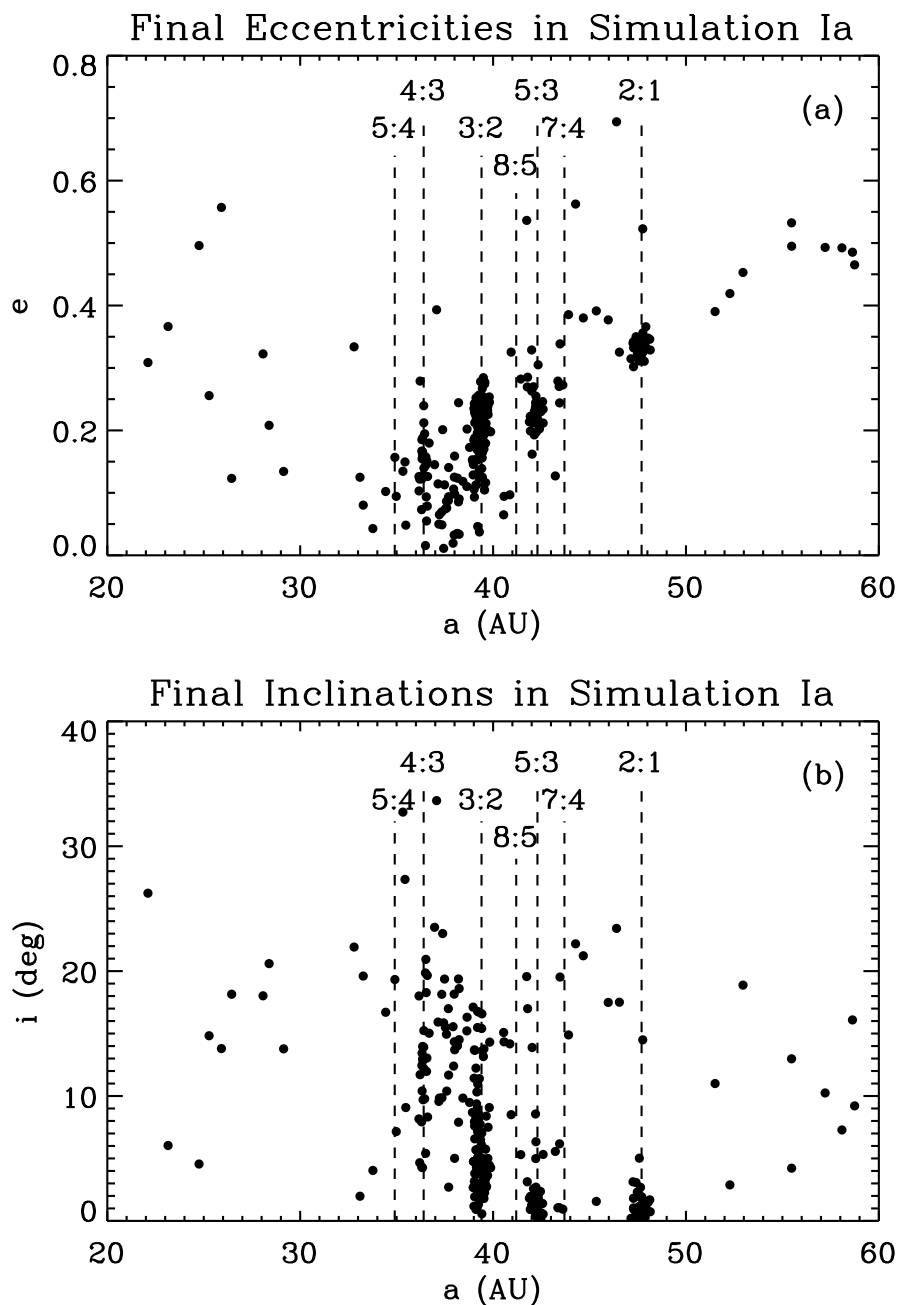


Fig. 3.— (a) Final eccentricities vs. semi-major axes for particles with $a \leq 60$ AU in simulation Ia for which $\tau = 10^7$ yr. (b) Final inclinations vs. semi-major axes. Out of 400 test particles potentially swept into the 3:2 resonance, 92 are actually captured. Of these 92, perhaps only 42 would remain bound to the 3:2 resonance over the age of the solar system.

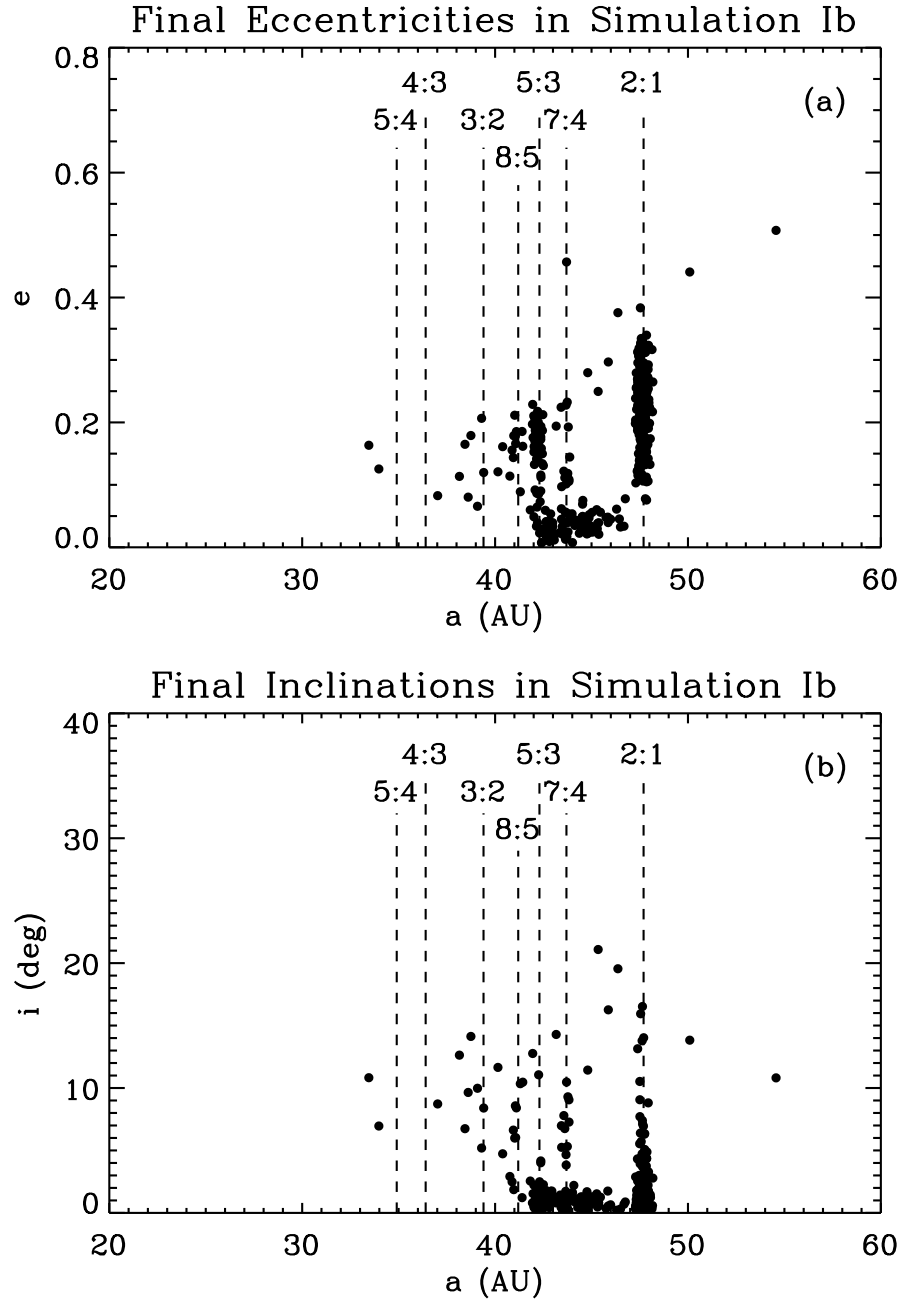


Fig. 4.— (a) Final eccentricities vs. semi-major axes for particles with $a \leq 60$ AU in simulation Ib for which $\tau = 10^7$ yr. (b) Final inclinations vs. semi-major axes. Out of 400 test particles potentially swept into the 2:1 resonance, 212 are actually captured. Of these 212, perhaps ~ 100 would remain bound to the 2:1 resonance over the age of the solar system.

explaining the inclination distribution of Plutinos has been noted by Brown (2001). We note further that 4 out of the 5 observed Twotino candidates have orbital inclinations between 11.8° and 13.5° —values characteristically larger than what the migration model predicts for objects in the 2:1 resonance.

3.3. Libration Statistics and Retainment Efficiencies

For the Plutinos in simulation Ia, we find that $\langle \Phi_{3:2} \rangle = \pi$, as expected from resonant perturbation theory for low eccentricity orbits. The distribution of libration amplitudes, $\Delta\Phi_{3:2} \equiv [\max(\Phi_{3:2}) - \min(\Phi_{3:2})]/2$, is supplied in Figure 6. Most objects have substantial libration amplitudes $\gtrsim 1$ rad. Levison & Stern (1995) and Morbidelli (1997) calculate that Plutinos having large $\Delta\Phi$ can escape the 3:2 resonance over the age of the solar system. Thus, many of the Plutinos that are captured in our simulation Ia would not likely survive if we were to extend our integration to $t_f^{\text{Ia}} = 4 \times 10^9$ yr. We define the retainment efficiency, $g_{3:2}$, to be the fraction of captured Plutinos that either have $\Delta\Phi < 110^\circ$ or that exhibit libration of ω about $\pm 90^\circ$. These selection criteria are motivated by the stability study of Levison & Duncan (1995; see their Figure 7). Of the 92 captured Plutinos in simulation Ia, 42 satisfy our criteria for long-term residency; the resultant value for $g_{3:2} = 46\%$ is recorded in Table 1.

For the Twotinos in simulation Ib, $\langle \Phi_{2:1} \rangle$ groups about 3 values: $\sim\pi/2$, π , and $\sim 3\pi/2$. The splitting of libration centers at large e from a single center at π to two additional centers at $\sim\pi/2$ and $\sim 3\pi/2$ was explored by Morbidelli, Thomas, & Moons (1995), Malhotra (1996), and references therein. Figure 7 plots $\Delta\Phi_{2:1}$ against $\langle \Phi_{2:1} \rangle$. Objects that reside more deeply in the resonance librate about $\langle \Phi_{2:1} \rangle \approx 3\pi/2$ and $\pi/2$. The former center is more heavily populated than the latter at the level of 93 to 85 objects. Though this difference is formally statistically insignificant, we nonetheless believe that it reflects a heretofore unnoticed and physically significant signature of the migration model. Further evidence supporting our contention is provided in §4, where we demonstrate that faster migration speeds dramatically enhance the asymmetry to levels of statistical significance. Unlike for the case of the 3:2 resonance, long-term, systematic studies of the stability of objects within the 2:1 resonance have not been published. It might be thought that the requirements for stability within the 2:1 resonance are less stringent than for the 3:2 resonance, because the ν_8 and ν_{18} secular resonances do not overlap the 2:1 (Morbidelli et al. 1995). Simulations by Malhotra (2002, personal communication) indicate that the retainment efficiency is roughly $g_{2:1} = 50\%$, and we will adopt this value in this paper.

Many of the objects having $\langle \Phi_{2:1} \rangle \equiv [\max(\Phi_{2:1}) + \min(\Phi_{2:1})]/2 \approx \pi$ also librate from

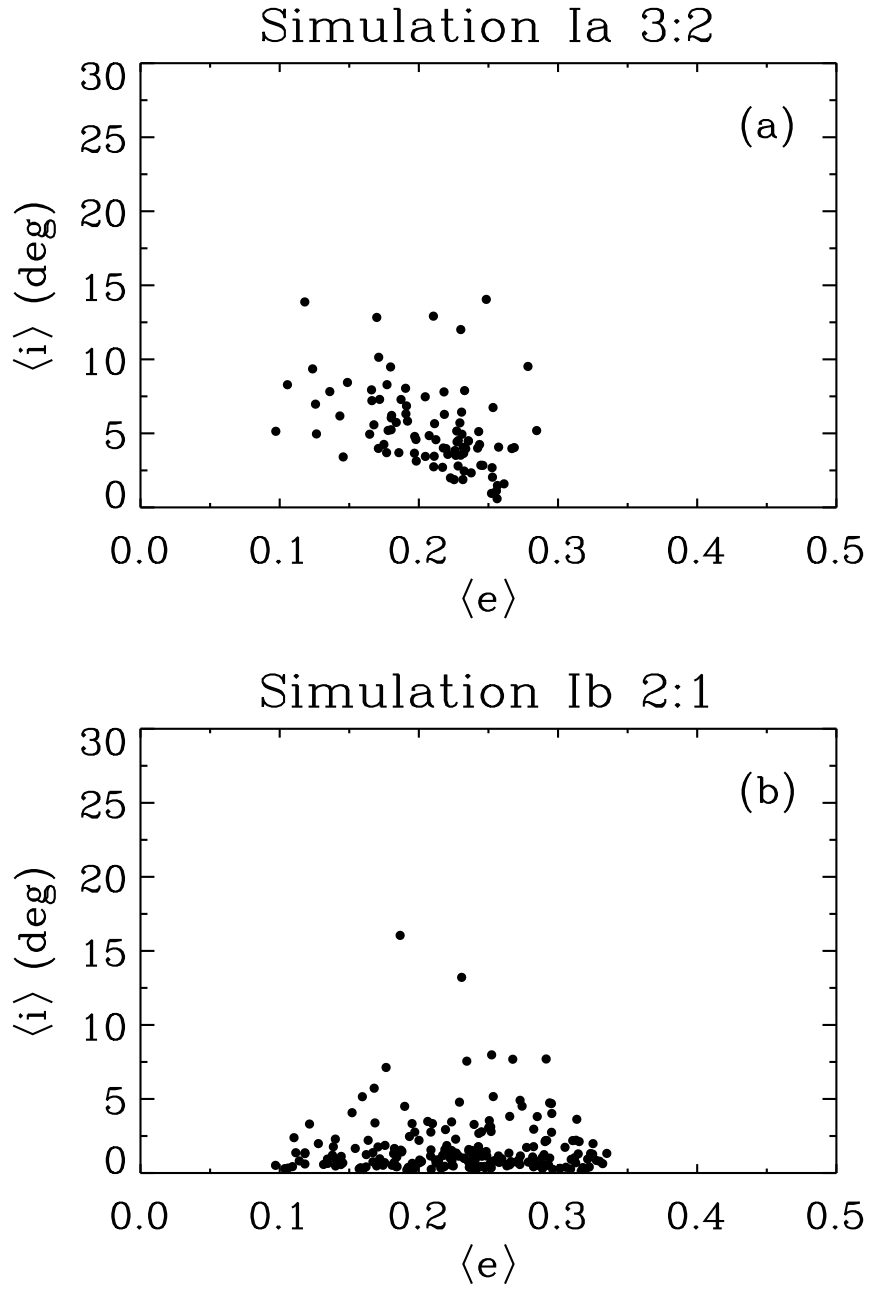


Fig. 5.— (a) Average i vs. average e of Plutinos during the final 1×10^7 yr of simulation Ia, after the planets effectively cease to migrate. (b) Average i vs. average e of Twotinos during the final 3×10^7 yr of simulation Ib. While $\langle i \rangle$ and $\langle e \rangle$ for Plutinos tend to be inversely correlated, no such tendency exists for Twotinos.

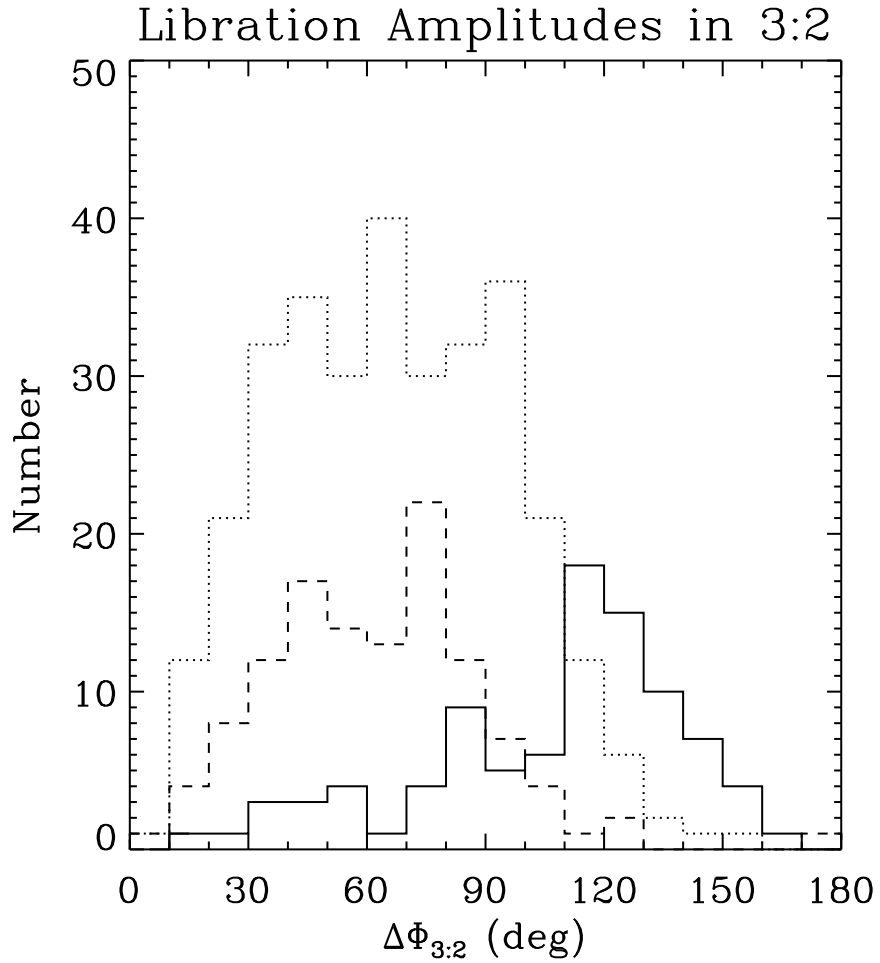


Fig. 6.— Distribution of libration amplitudes of captured Plutinos in simulation Ia (solid; $\tau = 10^7$ yr), IIa (dotted; $\tau = 10^6$ yr), and IIIa (dashed; $\tau = 10^5$ yr). Simulations IIa and IIIa are discussed in §4. Reducing τ below 10^7 yr yields smaller libration amplitudes and thus greater efficiencies of retainment of objects within the 3:2 resonance.

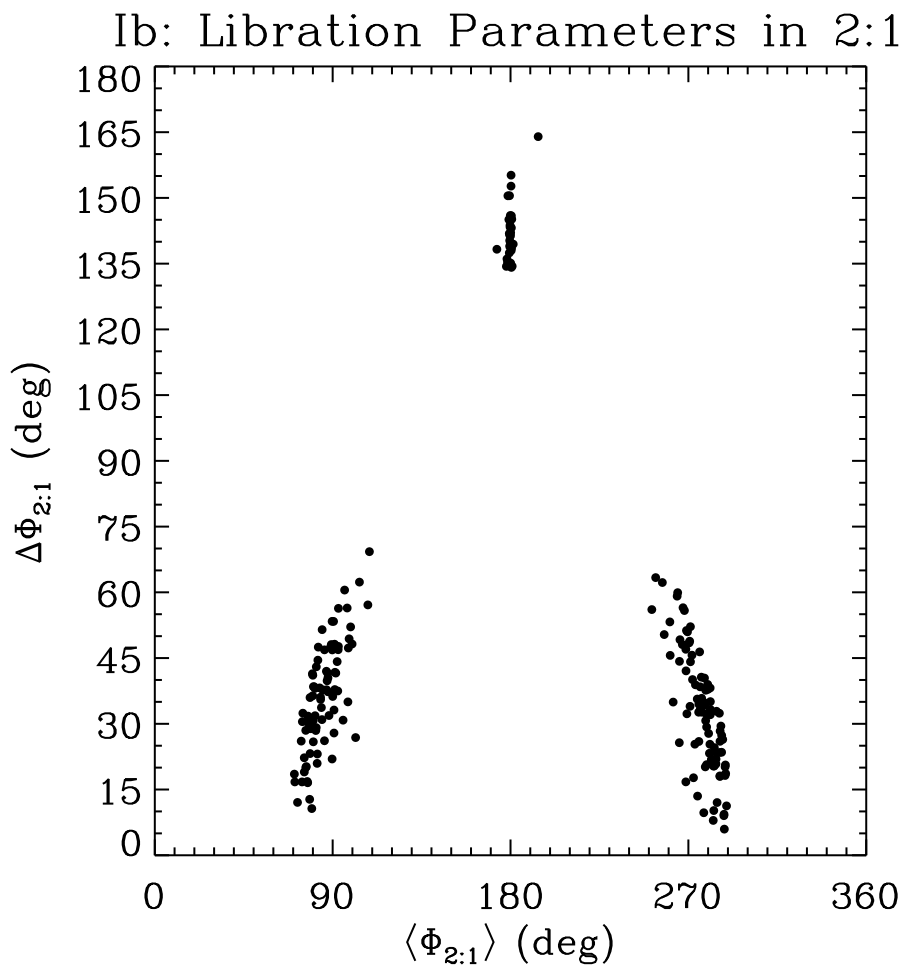


Fig. 7.— Amplitude of libration vs. libration center for Twotinos. The majority of Twotinos librate about $\langle \Phi_{2:1} \rangle \approx \pm\pi/2$ and have libration amplitudes that are smaller than those of Twotinos librating about $\langle \Phi_{2:1} \rangle = \pi$. The lobe at $\langle \Phi_{2:1} \rangle \approx 3\pi/2$ contains 10% more particles than the lobe at $\langle \Phi_{2:1} \rangle \approx \pi/2$; this asymmetry becomes more pronounced as shorter migration timescales are considered; compare with Figure 18.

time to time about $\sim\pi/2$ and $\sim3\pi/2$. An example of such a “three-timing” Twotino is displayed in Figure 8. A histogram of libration amplitudes of Twotinos is given in Figure 9.

For completeness, $\langle e \rangle$, $\langle i \rangle$, $\langle \Phi_{j+1:j} \rangle$, and $\Delta\Phi_{j+1:j}$ are plotted against one another in Figures 10 and 11. One correlation that emerges is that between $\langle e \rangle$ and $\langle \Phi_{2:1} \rangle$ for $\langle \Phi_{2:1} \rangle \approx \pi/2, 3\pi/2$. Increasing $\langle e \rangle$ increases the separation of the two principal libration centers away from $\langle \Phi_{2:1} \rangle = \pi$, an effect seen previously by Malhotra (1996). Another correlation appears between $\Delta\Phi_{3:2}$ and $\langle i \rangle$. Large amplitude librators tend to have large $\langle i \rangle$.

3.4. Capture into Secular Resonances

Of the 92 captured Plutinos in simulation Ia, 9–17 evince libration of ω over the last 1×10^7 yr of the simulation. Our uncertainty arises because for 8 Plutinos, the duration of the simulation is too short to see either a complete cycle of libration or of circulation. The libration centers, $\langle \omega \rangle$, are distributed over $\sim 90^\circ$, $\sim 180^\circ$, and $\sim 270^\circ$ for the 9 confirmed ω -librators. A sampling of the time evolution of ω for three ω -librators in the 3:2 resonance is provided in Figure 12.

Only a subset of the 92 captured Plutinos are likely to remain bound to the 3:2 resonance over 4×10^9 yr. Of the 92, we estimate that 42 are potential long-term residents: they either have $\Delta\Phi_{3:2} < 110^\circ$ or their ω 's librate with small amplitude about $\pm 90^\circ$ [compare with Levison & Stern (1995)]. Of these 42, 8–12 are ω -librators, or 20–30%. Since the ω -librators comprise a minority among surviving 3:2 resonant objects, and since $\langle \omega \rangle$ can equal 180° in addition to $\pm 90^\circ$, we conclude that secular libration of ω resulting from the migration model probably does not introduce strong latitudinal selection effects for the discovery of Plutinos. Of course, a zeroth-order assessment of latitudinal selection effects for resonant objects probably requires that we move beyond, or in the extreme case abandon, the model for resonant migration, since it apparently cannot reproduce very well the observed inclination distributions; see §3.2 and Brown (2001).

Similar conclusions are obtained for Twotinos. Of the 212 objects captured into the 2:1 resonance, only 12–15 evince libration of ω . Figure 13 samples three of them.

Our results address a question posed by Nesvorný, Roig, & Ferraz-Mello (2000; see their footnote 3). Could the observed paucity of Plutinos in the Kozai resonance today be a primordial relic of resonant capture and migration? Of the 42 captured Plutinos in simulation Ia that might survive in the 3:2 resonance over the age of the solar system, only 3–5 occupy a Kozai resonance for which $\langle \omega \rangle = 90^\circ$. This fraction of $\sim 4/42$ compares well with the observed fraction of $\sim 3/33$ reported by Nesvorný et al. (2000). Thus, our answer to their

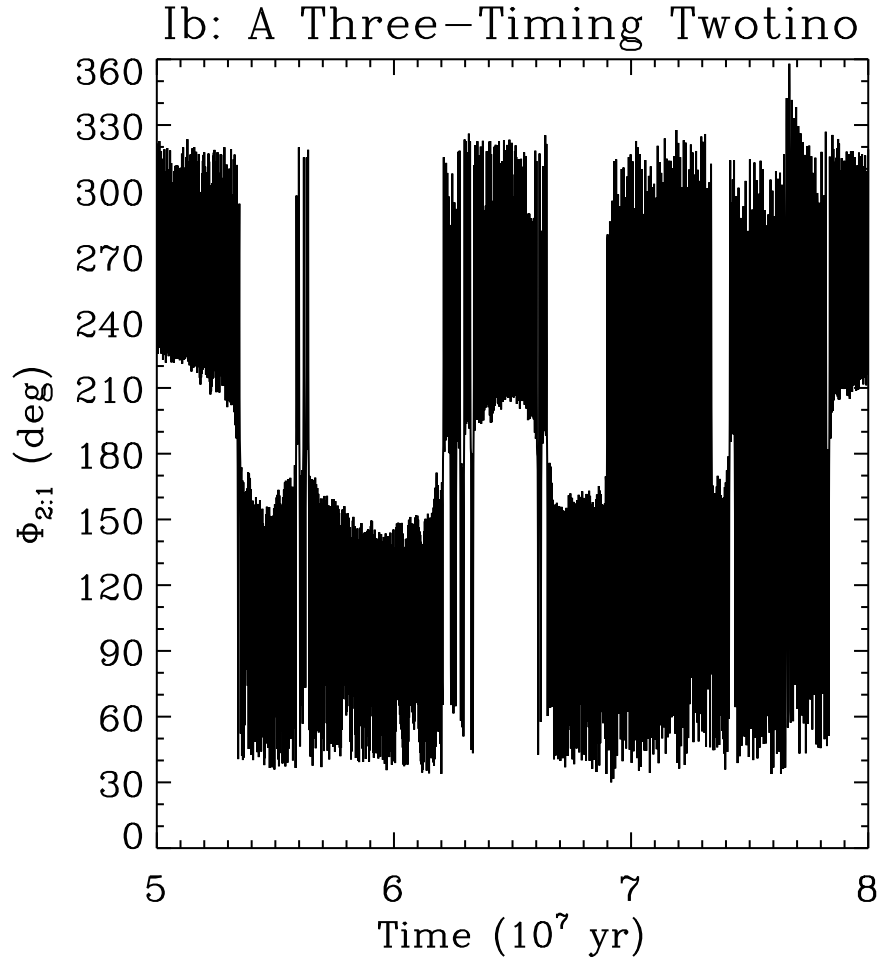


Fig. 8.— A Twotino that alternates between librating about $\langle \Phi_{2:1} \rangle \approx \pi/2, \pi,$ and $3\pi/2$.

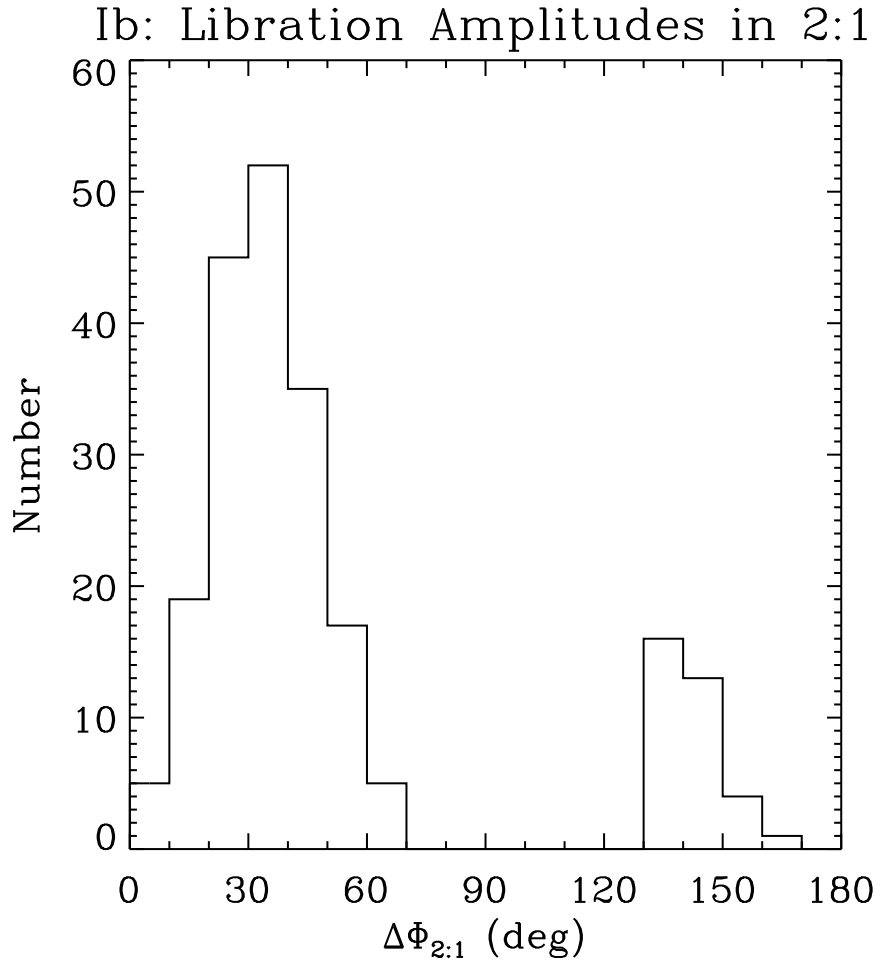


Fig. 9.— Distribution of libration amplitudes of Twotinos in simulation Ib.

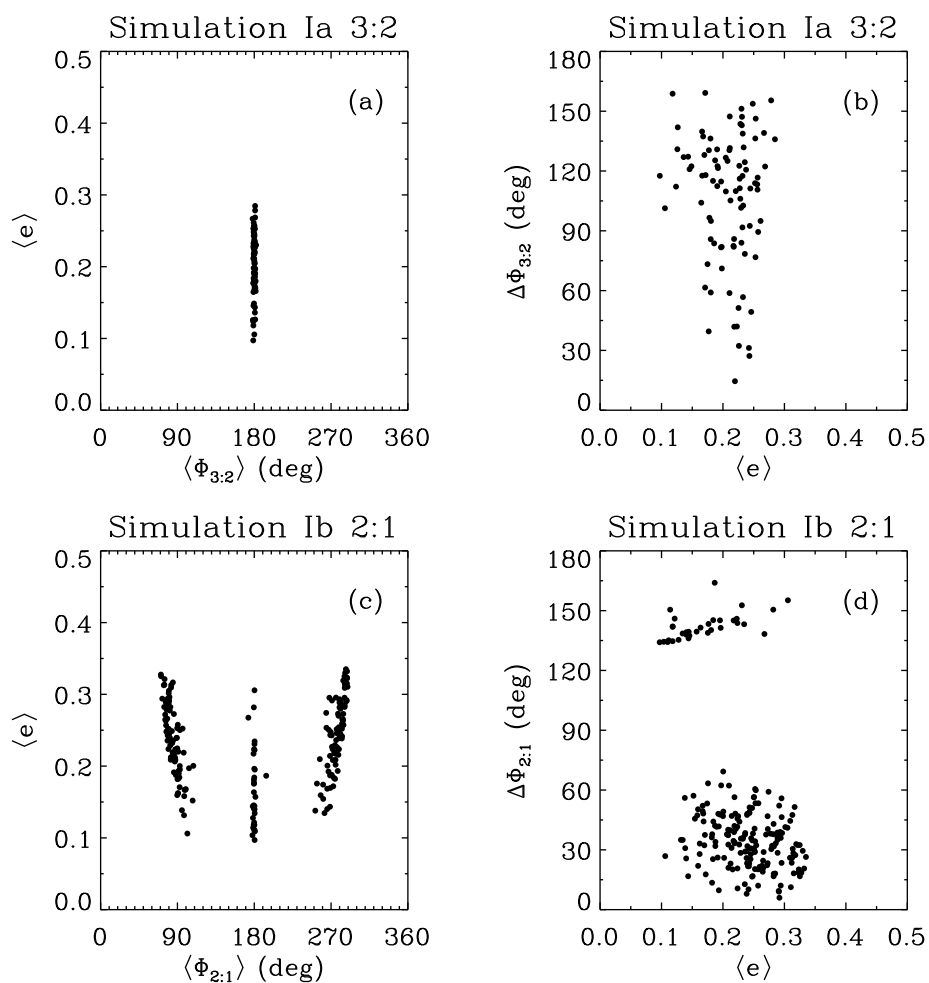


Fig. 10.— (a) Average e vs. average Φ for Plutinos. (b) Amplitude of libration vs. average e for Plutinos. (c,d) Same as (a,b) but for Twotinos. As seen in (c), Twotinos with higher eccentricities librate about centers closer to $\langle \Phi_{2:1} \rangle = 0^\circ$ than those with lower eccentricities.

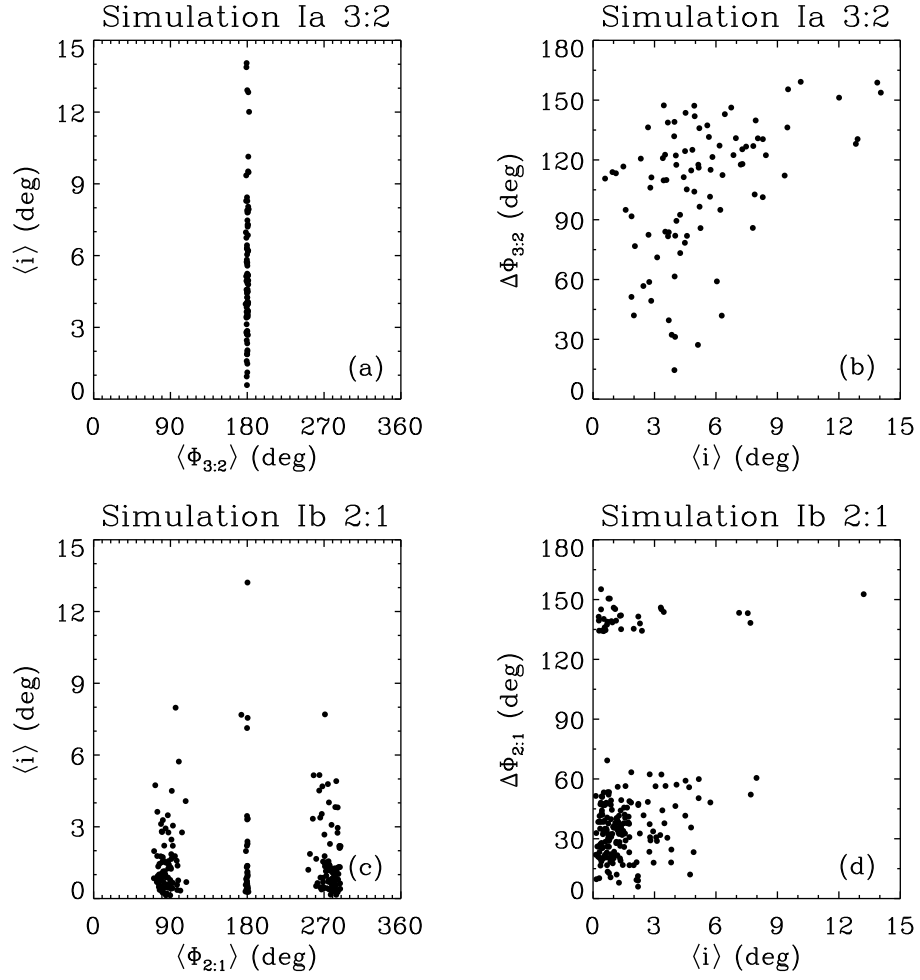


Fig. 11.— (a) Average i vs. average Φ for Plutinos. (b) Amplitude of libration vs. average i for Plutinos. (c,d) Same as (a,b) but for Twotinos. As seen in (b), highly inclined Plutinos tend to be weakly bound to the first-order, eccentricity resonance.

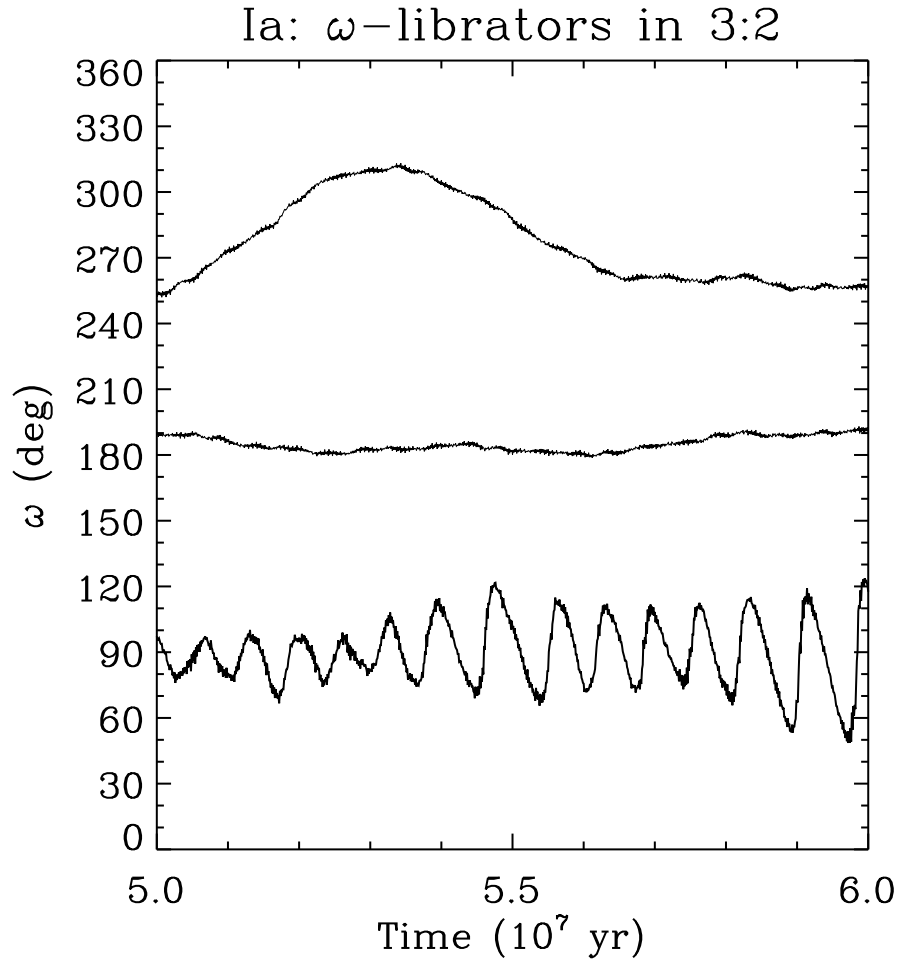


Fig. 12.— Time evolution of ω for three Plutinos that also inhabit Kozai-type resonances. Since the center of libration, $\langle\omega\rangle$, does not take a unique value, and since fewer than 30% of Plutinos are found in the simulation to be ω -librators, we conclude that Kozai-type resonances do not introduce strong latitudinal biases for finding Plutinos.

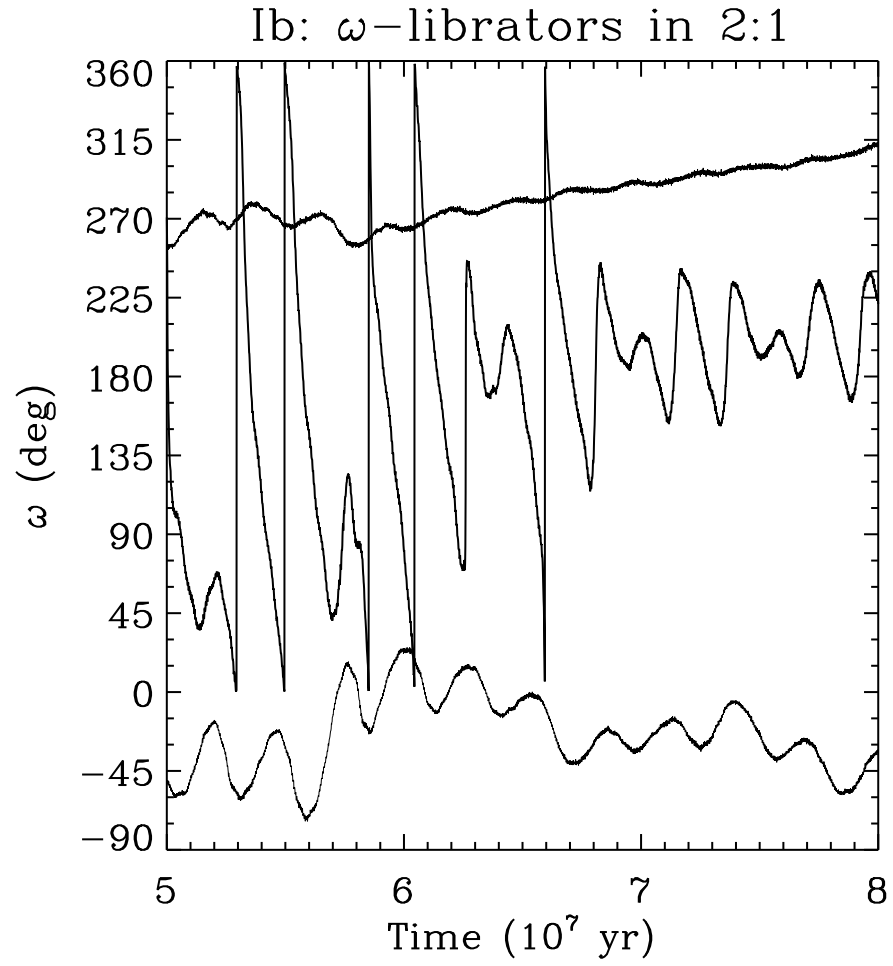


Fig. 13.— Time evolution of ω for three Twotinos in Kozai-type resonances. Fewer than 7% of the Twotinos in simulation Ib are ω -librators.

question is yes—scattering effects by Pluto need not be invoked to explain today’s observed low fraction of Plutinos in the Kozai resonance. We leave unaddressed two issues: (1) the effects of collisions amongst KBOs in the primordial belt in populating the Kozai resonance, and (2) whether the fact that the most massive Plutino yet discovered also inhabits the Kozai resonance is coincidental.

3.5. Spatial Distribution of Resonant Objects

We synthesize instantaneous snapshots of the spatial distribution of resonant objects from our simulation data as follows. Essentially, the positions of R resonant particles sampled at T different times are taken to represent the positions of $R \times T$ particles sampled at 1 time. Take the 2:1 resonance as an example. The inertial Cartesian coordinates of Neptune $[(x_N, y_N, z_N)]$ and of the $R = 212$ Twotinos $[(x_i, y_i, z_i), i = \{1, \dots, 212\}]$ at a time, t , in the simulation are rotated about the \hat{z} -axis by an angle

$$\Theta(t) = \arccos \frac{x_N(t)X_N + y_N(t)Y_N}{\sqrt{[x_N(t)^2 + y_N(t)^2](X_N^2 + Y_N^2)}}. \quad (4)$$

Here $X_N = 30.1 \cos(302^\circ)$ AU and $Y_N = 30.1 \sin(302^\circ)$ AU are the approximate current coordinates of Neptune. This procedure shifts the positions of all bodies into the Neptune-centric frame. We repeat this operation for T different instants of the simulation to generate T different snapshots. These snapshots are then overlaid on one another to yield a single image, a representation of the present-day spatial distribution of $R \times T$ resonant particles.

As noted in §3.3, only a subset of captured Plutinos will be retained by the 3:2 resonance over 4×10^9 yr. We employ the subset of $R = g_{3:2} \times f_{3:2} \times 400 = 42$ objects to construct the Plutino snapshot plot (Figure 14) and those figures quantifying the longitudinal variations of Plutino density (Figures 16a and 17).

Our method is not strictly justifiable if Neptune does not execute a perfectly circular orbit that remains in the invariable plane. In practice, Neptune’s eccentricity and inclination are so small that we do not consider this a serious violation. A more weighty concern is whether the true distributions of orbital elements—eccentricities, inclinations, and libration amplitudes—of $R \times T$ particles are well represented by only R particles. Since R is not small for either simulation, and since the distribution functions displayed in Figures 6, 7, 9, 10, and 11 do not betray poor coverage of phase space, we proceed with confidence.

Figures 14 and 15 showcase the present-day snapshots of Plutinos and Twotinos, respectively. For the former figure, $T = 1000$ time slices of $R = 42$ particles are sampled

uniformly between $t_1 = 5 \times 10^7$ yr and $t_2 = 6 \times 10^7$ yr; for the latter figure, $T = 190$, $R = 212$, $t_1 = 5.000 \times 10^7$ yr, and $t_2 = 5.190 \times 10^7$ yr. More time slices could be sampled for the Twotinos, but we restrict T to keep the plots legible. These snapshots resemble closely the toy models presented in Figures 1b and 2d; we conclude that (weak) correlations between orbital elements such as $\Delta\Phi_{2:1}$ and $\langle e \rangle$ —correlations that are missing from the toy models—do not significantly influence the organization of resonant populations.

Plutinos in the migration model cluster $\pm 90^\circ$ away from Neptune. Twotinos cluster $\pm 75^\circ$ away. Plutinos avoid longitudes near Neptune and longitudes that are 180° away from Neptune. Twotinos largely avoid longitudes near Neptune. Longitudinal variations in the density of resonant objects are quantified in Figure 16, where we plot the number of objects per degree in longitude, $N_{j+1:j}$, inside a heliocentric distance, r . In constructing Figure 16, we employ all available time slices ($T = 1000$ in simulation Ia and $T = 3000$ in simulation Ib), and then normalize the curves for $N_{j+1:j}$ so that the total population within each resonance, integrated over all longitudes, equals 10000 objects.

The sweet spots on the sky for finding resonant objects are sweetest—that is, the contrast between maximum object density and minimum object density is greatest—for small limiting r (e.g., $r \leq 40$ AU). In the large r limit, the maximum contrast in object density is $\sim 200\%$ for Plutinos and $\sim 40\%$ for Twotinos. Note that the two sweet spots for Twotinos differ in strength; the spot displaced by -75° from Neptune contains more objects than the spot displaced by $+75^\circ$, reflecting a greater population of objects librating about $\langle \Phi_{2:1} \rangle \approx 3\pi/2$ rather than $\sim \pi/2$. See §3.3 and §4 for more discussion of this asymmetry.

In Figure 17, we divide $N_{3:2}$ by $N_{2:1}$ to compute the longitudinal bias in finding Plutinos over Twotinos. Though the population of each resonance is normalized to the same number, many more Plutinos will be found than Twotinos at small r , simply because the 3:2 resonance is located closer than the 2:1. Most interestingly, however, there exists a special longitude interval between 210° and 240° (between -90° and -60° of Neptune’s longitude) where approximately equal numbers of Plutinos and Twotinos are expected to be found. Within this longitude interval, the yield of Twotinos to Plutinos ranges from 0.4 to 1 as the limiting r increases from 40 AU to ∞ (assuming that the two resonances are equally well populated). The absolute object density ($N_{j+1:j}$) for each resonance is also maximal over this longitude range, making this interval the sweetest of spots. A similar spot exists between 0° and 40° longitude ($+60^\circ$ – 100° of Neptune’s longitude); here $N_{2:1}/N_{3:2}$ varies from 0.3 to 0.9 as the limiting r increases from 40 AU to ∞ .

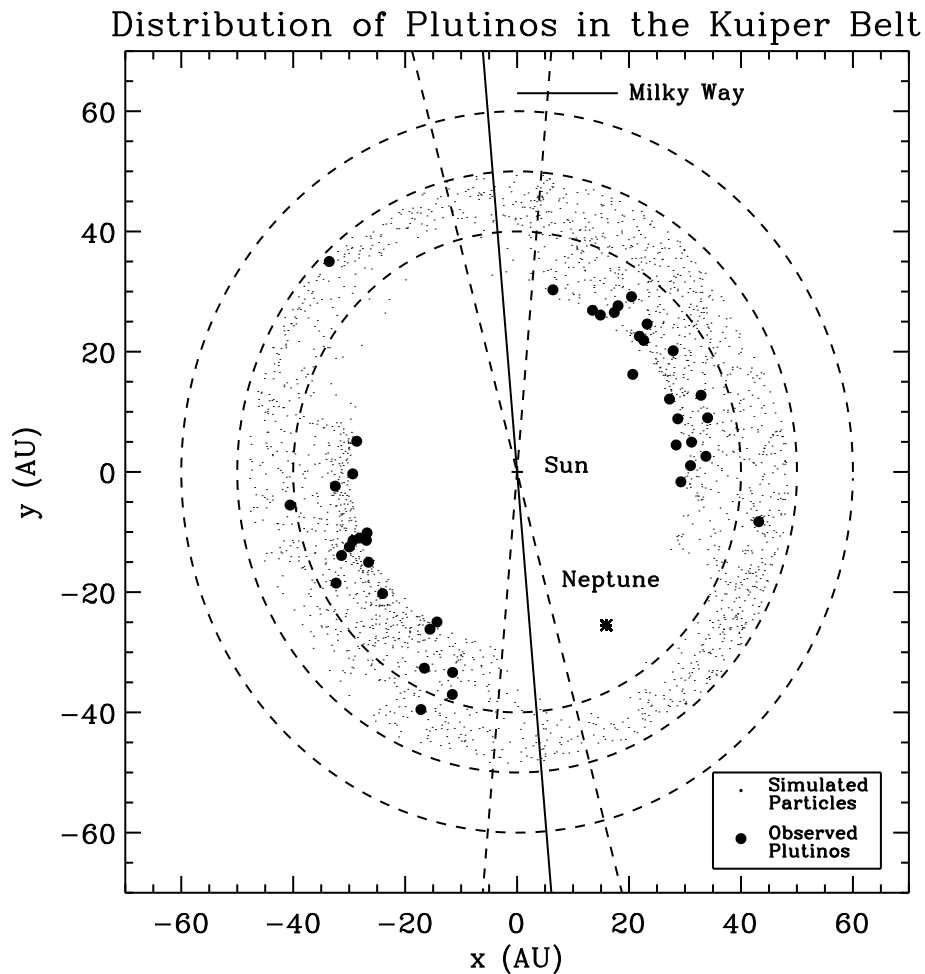


Fig. 14.— Synthesized snapshot, viewed from the invariable pole, of the spatial distribution of low libration amplitude Plutinos in simulation Ia, for which $\tau = 10^7$ yr. Large black dots mark the positions of observed Plutino candidates catalogued by the Minor Planet Center as of July 4, 2002. The main features of the snapshot, including the “sweet spot” concentrations of Plutinos displaced $\pm 90^\circ$ from Neptune’s longitude, and the relative dearth of Plutinos at longitudes 0° and 180° from Neptune’s, can be reproduced by a simple toy model; compare with Figure 1b. Dashed circles indicate heliocentric distances of 40, 50, and 60 AU. Radial lines delineate where the Galactic plane, $\pm 10^\circ$ Galactic latitude, intersects the invariable plane; Kuiper Belt surveys avoid the Galactic plane because fields there tend to be too crowded with stars.

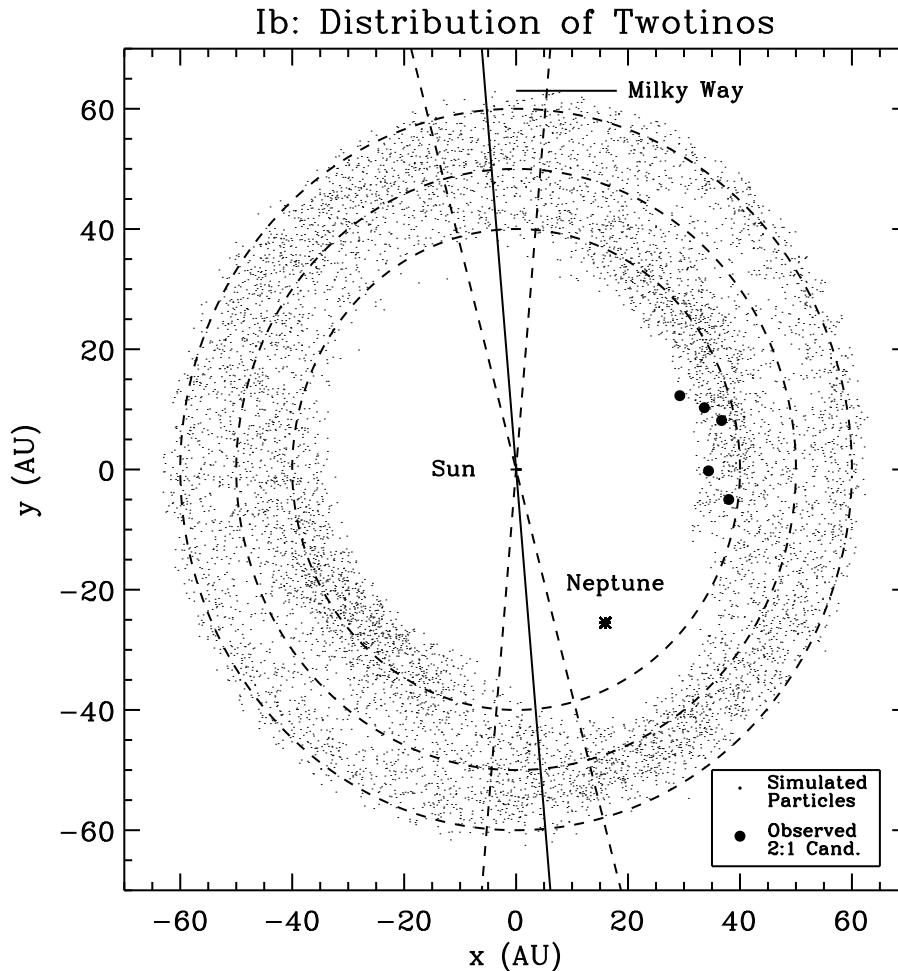


Fig. 15.— Synthesized snapshot, viewed from the invariable pole, of the spatial distribution of Twotinos subsequent to resonant capture in simulation Ib, for which $\tau = 10^7$ yr. Large black dots mark the positions of observed Twotino candidates catalogued by the Minor Planet Center as of July 4, 2002. The main features of the snapshot, including the “sweet spot” concentrations of Twotinos displaced $\pm 75^\circ$ from Neptune’s longitude, and the relative dearth of Twotinos at longitudes near those of Neptune, can be reproduced by a simple toy model; compare with Figure 2d. Dashed circles indicate heliocentric distances of 40, 50, and 60 AU, and radial lines delineate where the Galactic plane, $\pm 10^\circ$ Galactic latitude, intersects the invariable plane. Strangely, though the model predicts roughly equal numbers of Twotinos ahead and behind of Neptune’s longitude, Twotino candidates have only been detected in the former lobe. Contrast this snapshot with the one in Figure 19, where we consider a migration phase that is $10\times$ shorter.

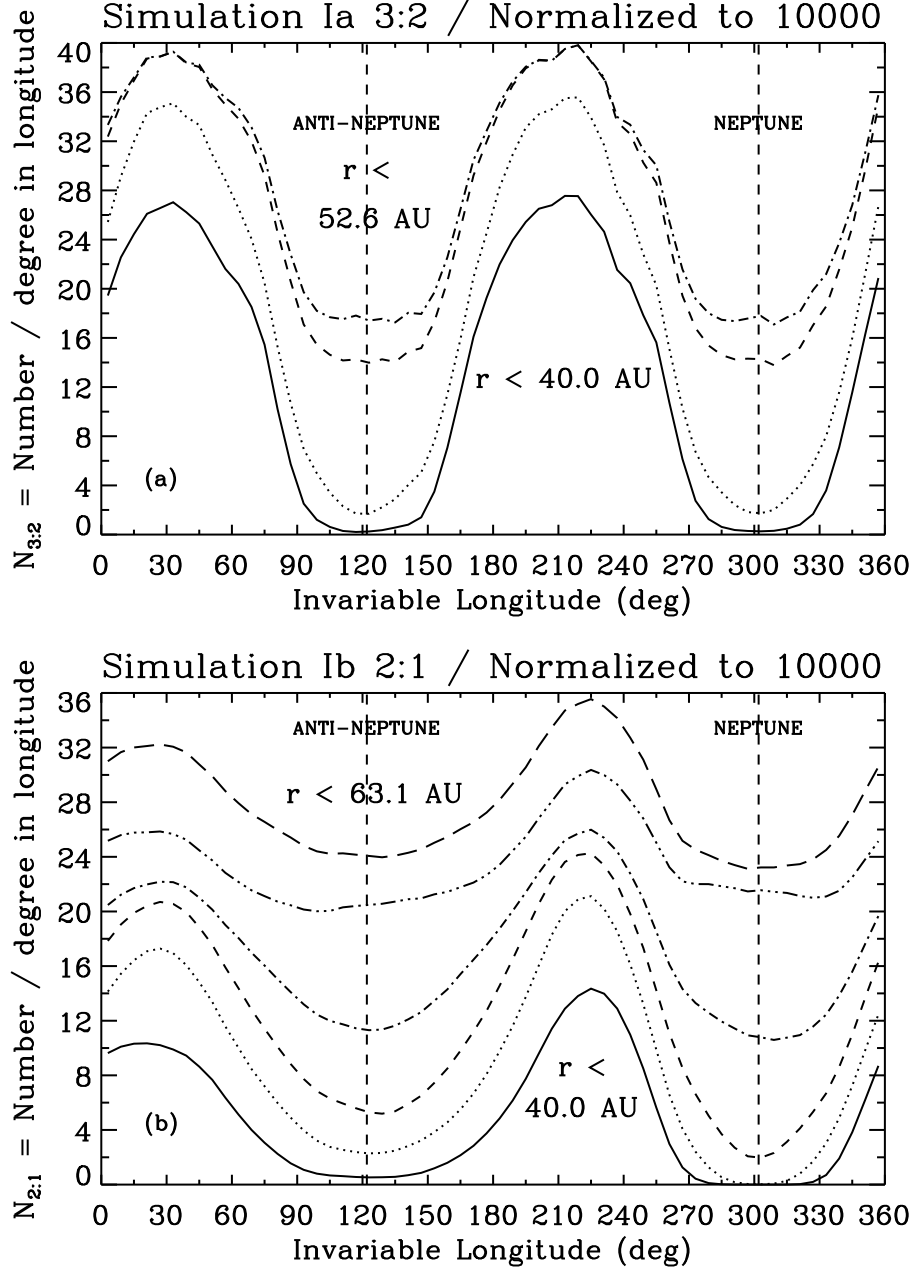


Fig. 16.— Longitudinal distribution of (a) Plutinos selected for likely long-term stability, and (b) Twotinos. Data are synthesized from simulation I, for which the migration timescale $\tau = 10^7$ yr. The number of objects within each resonance, integrated over all longitudes, is normalized to 10000. Each curve represents those objects located at heliocentric distances, r , less than the value shown. Adjacent curves differ by a multiplicative factor of 1.0955 in limiting r . Longitudes for Neptune and for the anti-Neptune direction are indicated. The contrast in object density from longitude to longitude is greatest at small limiting r . Plutinos cluster at longitudes $\pm 90^\circ$ away from Neptune, while Twotinos are most likely found $\pm 75^\circ$ away.

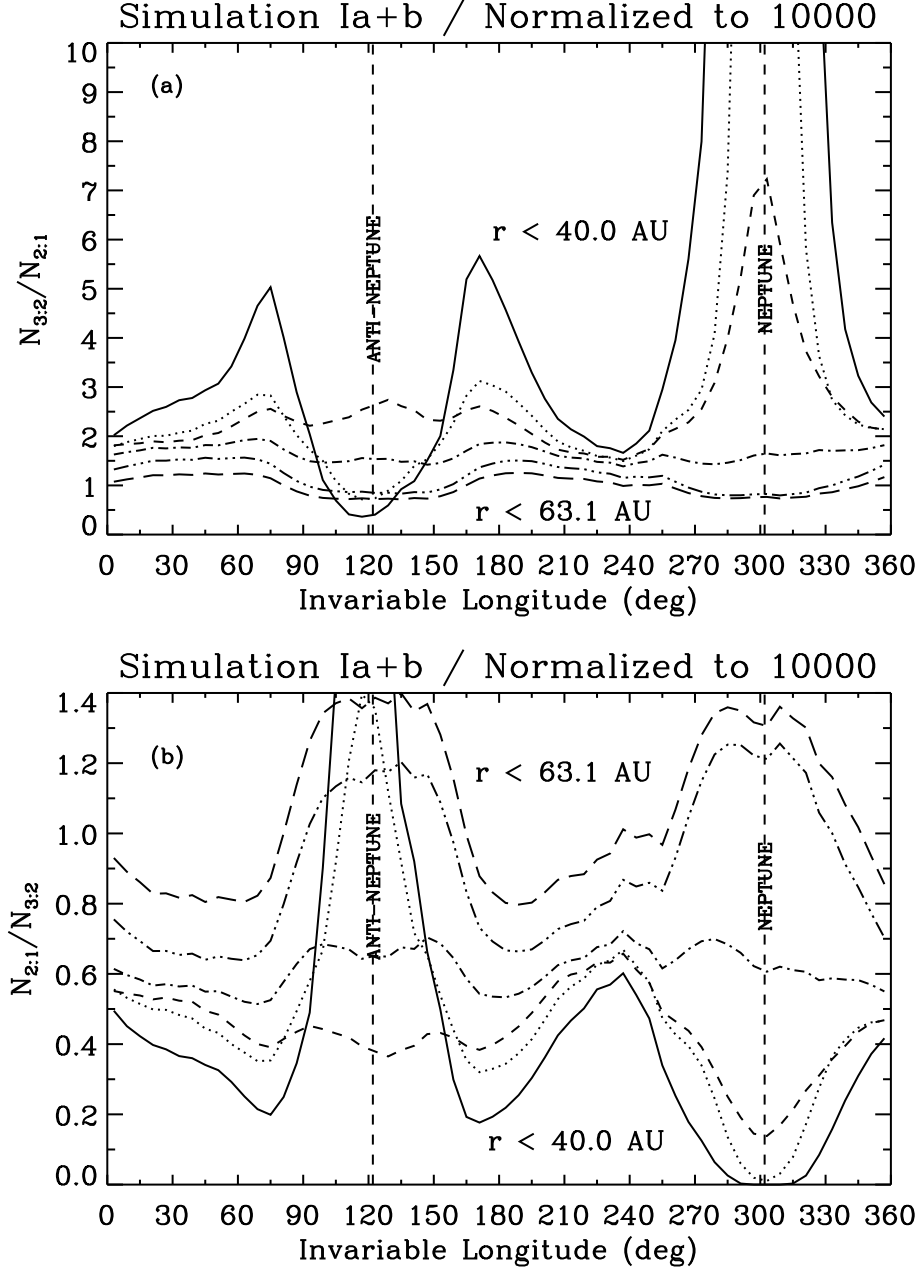


Fig. 17.— Longitudinal variations of the bias in finding Twotinos vs. Plutinos in simulation I, for which $\tau = 10^7$ yr. As in Figure 16, the number of objects in each resonance is normalized to 10000. Panel (a) plots the fraction of Plutinos to Twotinos found inside a heliocentric distance, r , while panel (b) plots the inverse ratio. Adjacent curves differ by a factor of 1.0955 in limiting r . At longitudes between 210° and 240° (between -90° and -60° of Neptune’s longitude), yields of Twotinos and Plutinos are expected to be nearly equal. A similar interval exists between 0° and 40° longitude ($+60^\circ$ – 100° of Neptune).

4. VARYING THE MIGRATION SPEED

Simulations IIa and IIb are identical to Ia and Ib, respectively, except that we set $\tau = 10^6$ yr and $t_f^{\text{II}} = 5 \times 10^6$ yr. For simulations IIIa and IIIb, $\tau = 10^5$ yr and $t_f^{\text{III}} = 5 \times 10^5$ yr.

Table 1 summarizes the computed capture efficiencies, f , and estimated retainment efficiencies, g , for each simulation. The retainment efficiency equals the fraction of captured objects that are expected to remain in the resonance over 4×10^9 yr. For Twotinos, we assume that $g = 0.5$ (see §3.3). For Plutinos, g equals the fraction of captured objects that either have $\Delta\Phi < 110^\circ$ or that librate about $\langle\omega\rangle = \pm 90^\circ$.

For $\tau = 10^6$ yr, $f_{2:1} \approx 15\%$, more than three times lower than the corresponding value for $\tau = 10^7$ yr. By contrast, $f_{3:2}(\tau = 10^6 \text{ yr}) \approx 78\%$, more than three times as high as $f_{3:2}(\tau = 10^7 \text{ yr})$ because fewer objects are lost to capture by the 2:1 or to close encounters with Neptune. For $\tau = 10^5$ yr, $f_{2:1} \approx 0\%$, while $f_{3:2} \approx 30\%$. Our results are consistent with those of Ida et al. (2000) and Friedland (2001).

The Plutinos’ distribution of libration amplitudes shifts substantially towards smaller values as τ is reduced. Figure 6 plots histograms of $\Delta\Phi_{3:2}$ for all three simulations, Ia, IIa, and IIIa. Table 1 records how the retainment efficiency, g , more than doubles for Plutinos as τ is reduced from 10^7 yr to 10^6 yr, a consequence of the smaller libration amplitudes that characterize faster migration rates.

Remarkably, objects fill the 2:1 resonance asymmetrically: captured Twotinos prefer to librate about $\langle\Phi_{2:1}\rangle \approx 270^\circ$ rather than $\langle\Phi_{2:1}\rangle \approx 90^\circ$. Figure 18 plots $\Delta\Phi_{2:1}$ against $\langle\Phi_{2:1}\rangle$ for simulation IIb. The preferential filling of one resonance lobe over another dramatically affects the spatial distribution of Twotinos, as illustrated by Figure 19 and as quantified in Figure 20. The difference in populations is at the level of 330% and is statistically significant.² Establishing the relative populations of Twotinos ahead and behind of Neptune would offer a powerful constraint on the migration history of that planet.

Figure 21 is appropriate for $\tau = 10^6$ yr and is analogous to Figure 17.

²We have verified that for $\tau = 3 \times 10^6$ yr, the sign of the asymmetry remains the same and its magnitude is statistically significant and intermediate between that of simulations Ib and IIb—among the 141/400 objects captured into the 2:1 resonance, $3 \times$ as many Twotinos librate about $\langle\Phi_{2:1}\rangle \approx 270^\circ$ than about $\langle\Phi_{2:1}\rangle \approx 90^\circ$.

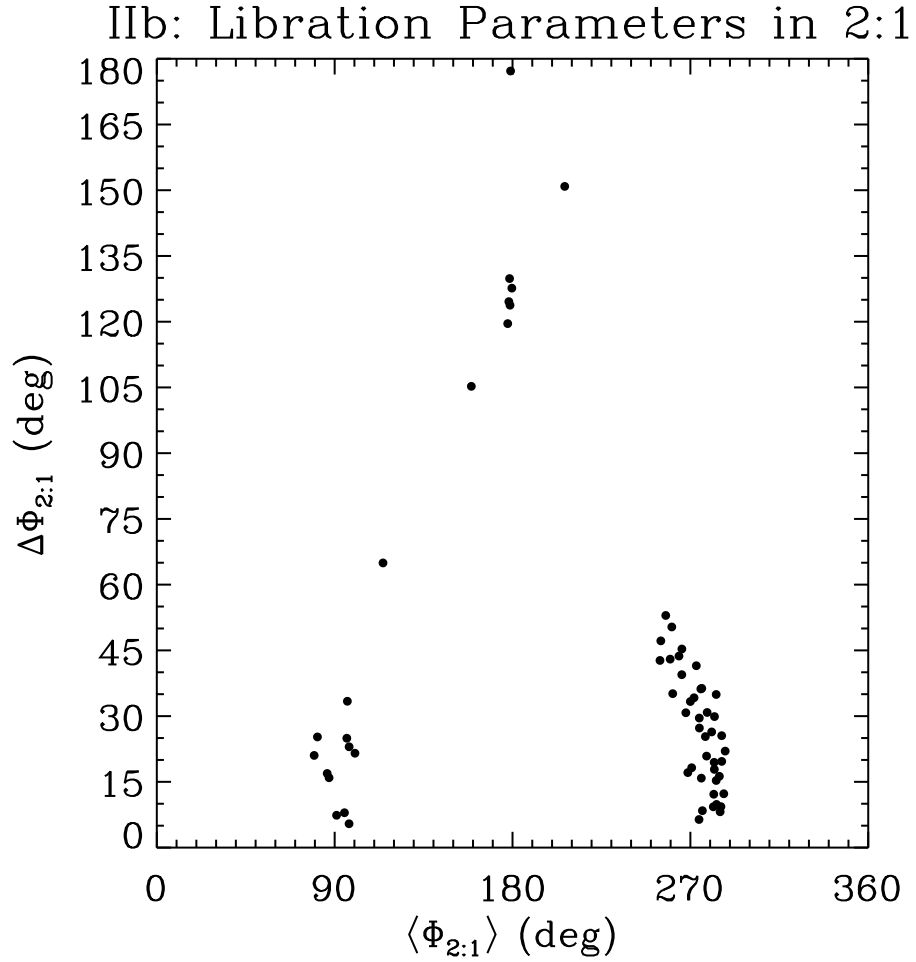


Fig. 18.— Amplitude of libration vs. libration center for Twotinos in simulation IIb, for which $\tau = 10^6$ yr. The lobe at $\langle \Phi_{2:1} \rangle = 270^\circ$ boasts greater membership than the lobe at $\langle \Phi_{2:1} \rangle = 90^\circ$ by a factor of 3.3-to-1. Contrast this result with Figure 7, for which $\tau = 10^7$ yr.

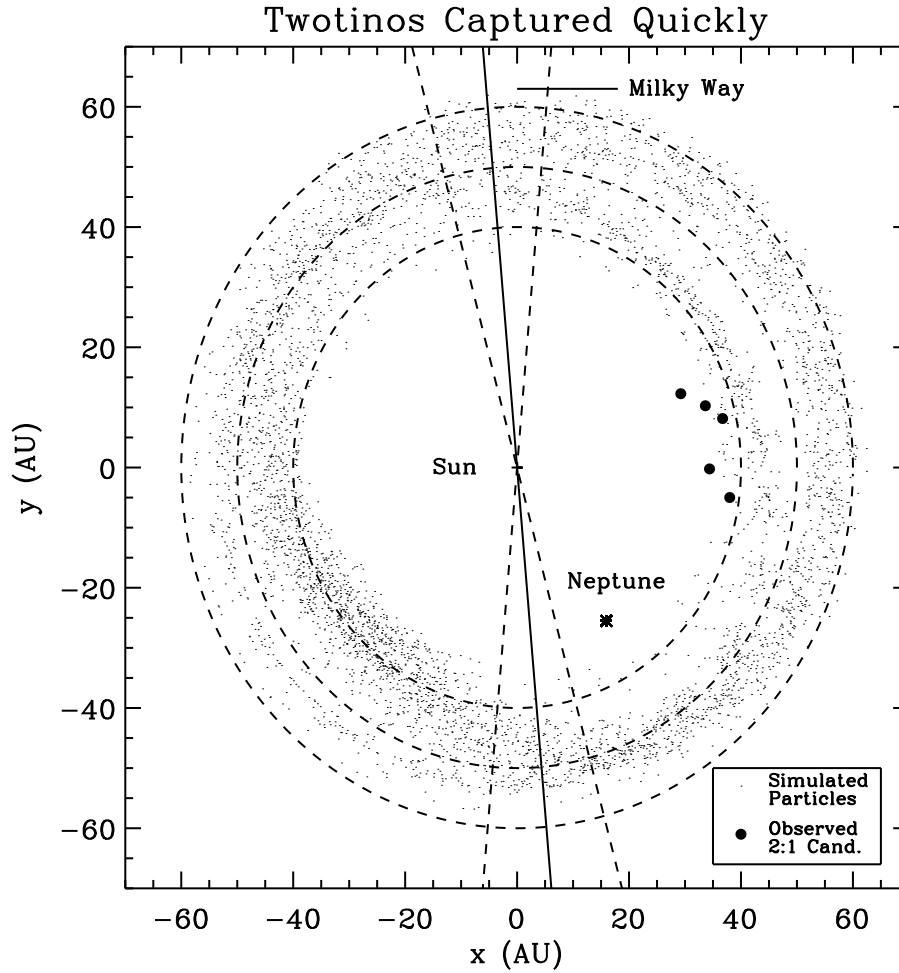


Fig. 19.— Snapshot of the spatial distribution of Twotinos in simulation IIb, viewed from the invariable pole. Large black dots represent observed Twotino candidates catalogued by the Minor Planet Center as of July 4, 2002. The shorter migration timescale of $\tau = 10^6$ yr leads to a pronounced asymmetry of objects in space. Dashed circles delimit heliocentric radii of 40, 50, and 60 AU, and radial lines indicate the intersection of the Galactic plane with the invariable plane.

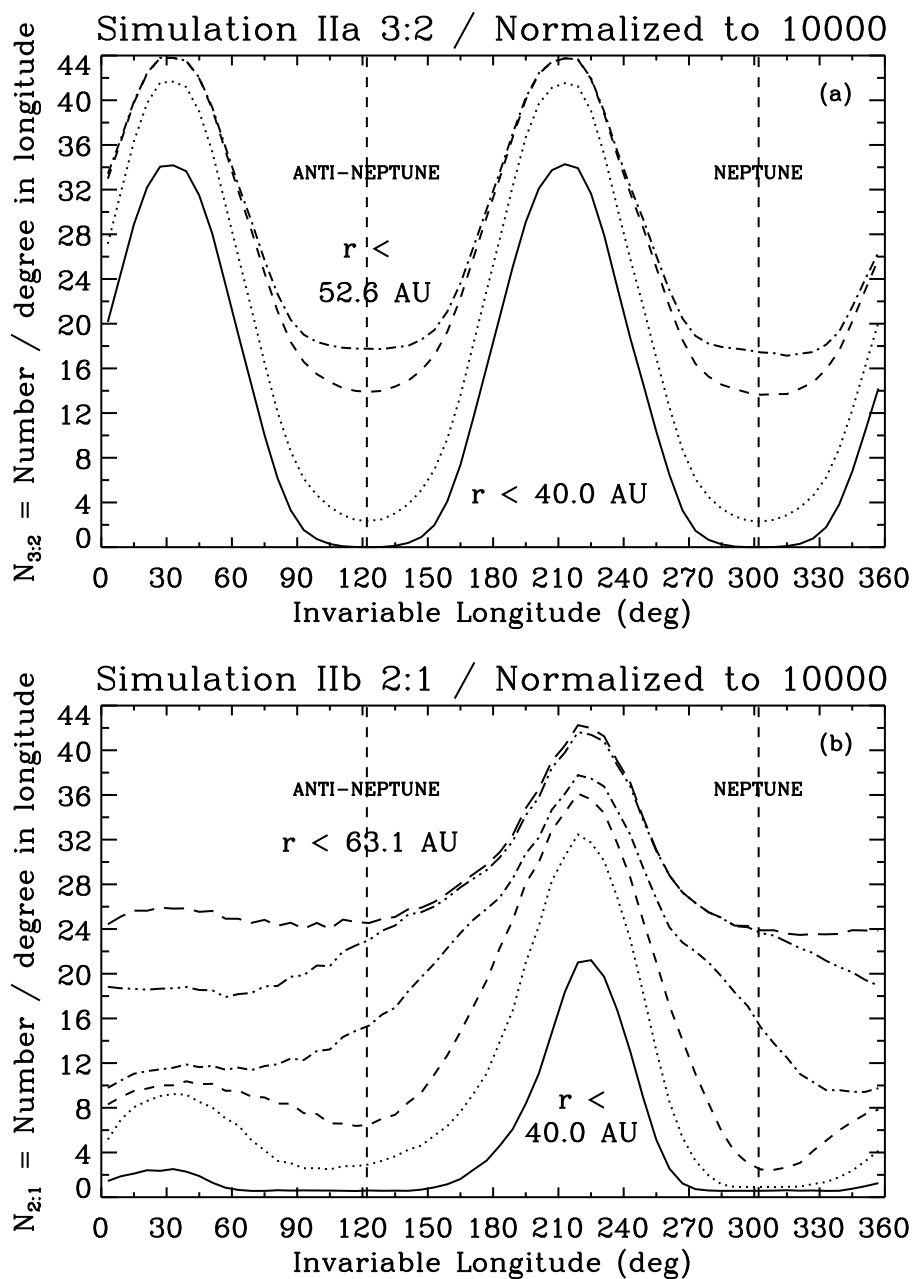


Fig. 20.— Longitudinal distribution of (a) Plutinos and (b) Twotinos in simulation II for which $\tau = 10^6$ yr. The curves are normalized so that each resonance contains 10000 objects; adjacent curves differ by a factor of 1.0955 in limiting r . For Twotinos, the sweet spot located -75° away from Neptune’s longitude is substantially sweeter than the one at $+75^\circ$. Compare with Figure 16 which portrays the results of simulation I for which $\tau = 10^7$ yr.

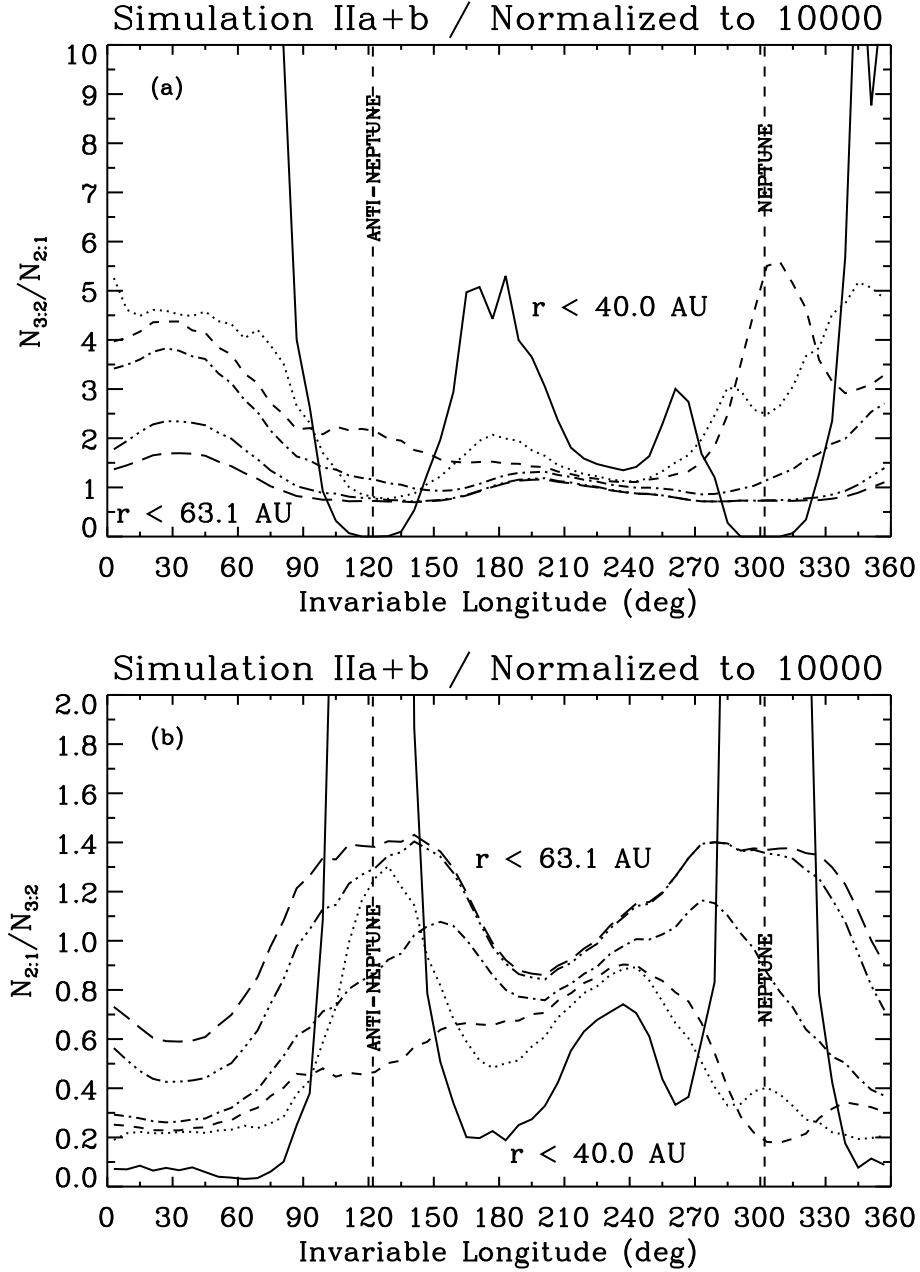


Fig. 21.— Longitudinal variations of the bias in finding Twotinos vs. Plutinos in simulation II, for which $\tau = 10^6$ yr. As in Figure 20, the number of objects in each resonance is normalized to 10000. By contrast with simulation I for which $\tau = 10^7$ yr, only the interval between 210° and 240° longitude (-90° to -60° of Neptune’s longitude) exhibits minimal bias in favor of detecting Plutinos over Twotinos; there, the yield of 3:2 resonant objects over 2:1 resonant objects ranges from 1 to 2.5 as the limiting heliocentric distance, r , out to which objects are detected increases from 40 AU to ∞ .

5. DISCUSSION

Under the hypothesis of resonant capture, the number of Plutinos having diameters greater than s , divided by the number of similarly sized Twotinos, is given today by

$$F(\gtrsim s, \tau) \equiv \frac{f_{3:2}(\tau) g_{3:2}(\tau) \eta_0(\gtrsim s, a \approx 35 \text{ AU})}{f_{2:1}(\tau) g_{2:1}(\tau) \eta_0(\gtrsim s, a \approx 42 \text{ AU})}. \quad (5)$$

Here $\eta_0(\gtrsim s, a)$ equals the number of objects having diameters greater than s that occupied an annulus of heliocentric radius a and radial width ≈ 8 AU just prior to the era of Neptune’s migration. From our findings in this paper, $(f_{3:2}g_{3:2})/(f_{2:1}g_{2:1})$ equals 0.40, 9.6, and ∞ for τ (yr) = 10^7 , 10^6 , and 10^5 , respectively (see Table 1).

We interpret the observation that the 2:1 resonance today contains at least one (candidate) object having a large eccentricity to imply that the migration timescale, τ , cannot be as low as 10^5 yr. More refined estimates of τ can be made by measuring the relative number of Twotinos whose resonant arguments $\langle \Phi_{2:1} \rangle$ librate about $\sim 3\pi/2$ rather than about $\sim \pi/2$; i.e., the relative number of Twotinos observed to reach perihelion at longitudes behind of as opposed to in front of Neptune’s longitude.

Estimates for the intrinsic F cannot be established without first de-biasing F_{obs} . As Figures 17 and equation (5) attest, F_{obs} depends not only on τ and the ratio of primeval populations, $\eta_0(a \approx 35 \text{ AU})/\eta_0(a \approx 42 \text{ AU})$, but also on (1) the longitude of observation, (2) the limiting magnitude of the observation, (3) the relative size distributions of Twotinos and Plutinos, (4) the relative albedo distributions, (5) the relative inclination distributions, and, because of consideration (5), (6) the latitude of observation. For purposes of discussion, let us assume that Plutinos and Twotinos follow the same size, albedo, and inclination distributions, so that we can focus on considerations (1) and (2) exclusively.

Roughly speaking, most KBOs have been detected by surveys having limiting magnitudes $m_V \sim 24$ (Millis et al. 2002; see also the survey statistics compiled in Chiang & Brown 1999). For this limiting magnitude, all objects that are inside $r \approx 44$ AU and that have sizes $s \gtrsim 200$ km and albedos $\gtrsim 0.04$ would be detected. These sizes and albedos are comparable to those estimated by the Minor Planet Center. Moreover, a glance at Figures 14 and 15 reveals that indeed, all but one of the observed Plutino and Twotino candidates have been discovered at $r < 44$ AU.

Thus, if we assume that $\tau = 10^7$ yr, and take the dotted curve for $r \leq 44$ AU in Figure 17 as our guide, then we crudely estimate the bias in finding Plutinos over Twotinos, averaged over all longitudes for which Plutinos have been discovered (330° – 90° , and 150° – 270°), to

be $N_{3:2}/N_{2:1} \sim 2.2$. Then the observed ratio, $F_{obs} \sim 8$, should be de-biased down to values closer to $8/2.2 \sim 3.6$. We emphasize that this is a model-dependent estimate of F that assumes that $\tau = 10^7$ yr. Since $(f_{3:2}g_{3:2})/(f_{2:1}g_{3:2})|_{\tau=10^7 \text{ yr}} \approx 0.40$, we would estimate the ratio of primeval populations to be $\eta_0(a \approx 35 \text{ AU})/\eta_0(a \approx 42 \text{ AU}) \sim 3.6/0.40 \sim 9$. This would reflect a steep drop in mass density over a short distance in the ancient planetesimal disk. Nonetheless, it would be consonant with the idea that a “Kuiper Cliff” (Chiang & Brown 1999; see also Allen, Bernstein, & Malhotra 2001; Jewitt, Luu, & Trujillo 1998; Gladman et al. 1998) delineates the edge of the classical Kuiper Belt at $a \approx 48 \text{ AU}$.

If we assume instead that $\tau = 10^6$ yr and repeat the same analysis by using the dotted line for $r \leq 44 \text{ AU}$ in Figure 21, we estimate an intrinsic $F \sim 8/3.0 \sim 2.7$, and a corresponding ratio of primeval populations of $\eta_0(a \approx 35 \text{ AU})/\eta_0(a \approx 42 \text{ AU}) \sim 2.7/9.6 \sim 0.3$. Thus, while our estimate that Plutinos intrinsically outnumber Twotinos by a factor of ~ 3 -to-1 seems robust to changes in τ , a dramatic drop in mass density with distance in the primordial planetesimal disk is by no means an assured conclusion.

The above estimates for F are plagued by other observational biases that are difficult to quantify. For example, the Minor Planet Center dataset probably contains more Plutinos relative to Twotinos than it should because (1) MPC orbit fitting algorithms for objects discovered a few AU inside Neptune’s orbit and having short astrometric arcs favor Plutino-like orbits as trial solutions (B. Marsden 2002, personal communication), and (2) the astrometric recovery rate of Plutinos is probably higher than that of Twotinos because the former objects are, on average, closer and therefore easier to re-detect by virtue of their brightness and large apparent proper motion. Both these factors lead us to conclude that our above estimates for F should be considered upper limits.

Superior estimates for F can be obtained by coupling our theoretical calculations to the results of surveys having well-documented discovery statistics and minimal bias in their algorithms for orbit fitting. The Deep Ecliptic Survey (DES; Millis et al. 2002), for example, promises to be one such survey; it employs the more objective method of Bernstein & Khushalani (2000) in fitting orbits with short arcs. We defer analysis of the resonant populations using their large and homogeneous dataset to future study.

An early but intriguing comparison between theory and observation lies in the complete absence of observed Twotino candidates at longitudes behind that of Neptune (see Figures 15 and 19). By contrast, our numerical experiments demonstrate that resonant capture and migration preferentially fill the 2:1 resonant lobe displaced behind of, rather than ahead of, Neptune’s longitude. Moreover, this asymmetry is only enhanced by faster rates of migration (Figure 19). With only ~ 5 candidate Twotinos, the probability of finding all of them in the forward lobe and not the backward lobe is $1/32$, under the prior that a Twotino is as likely

to be found in one lobe as the other. Whether the actual Kuiper Belt defies the predicted sign of the asymmetry—in which case the present theory of resonant capture and migration must be considered either incomplete or incorrect—only continuing surveys for KBOs will tell.

6. SUMMARY

We have analyzed quantitatively the predictions of the model of resonant capture and migration for the 2:1 (Twotino) and 3:2 (Plutino) populations of the Kuiper Belt. We summarize our main findings as follows:

1. The instantaneous spatial distribution of resonant objects depends not only on the libration centers of their resonant arguments, $\langle\Phi\rangle$, but also on their distribution of libration amplitudes, $\Delta\Phi$. For example, if $\Delta\Phi \gtrsim 1$ rad for most Plutinos, the usual expectation that such objects are most readily found $\pm 90^\circ$ away from Neptune’s longitude would not be valid. The distribution of libration amplitudes within a given resonance is model-dependent.
2. We have numerically evaluated the capture efficiencies, f , of the sweeping 2:1 and 3:2 resonances for three values of the migration timescale, $\tau(\text{yr}) = 10^7, 10^6$, and 10^5 . The timescale is assumed to be one of exponential decay. We define the capture efficiency to equal the fraction of objects whose orbits are initially spread uniformly over the complete path of a given sweeping resonance and that are ultimately captured by it. This efficiency depends not only on the probability of capture into the isolated resonant potential of interest, but also on the probability of pre-emptive capture into other resonances that lie exterior to the given resonance, and on the probability of violent scattering by close encounters with the planets. The capture efficiency for Twotinos, $f_{2:1}$, decays from 53% to 0% as τ is reduced from 10^7 yr to 10^5 yr. The capture efficiency for Plutinos, $f_{3:2}$, increases from 23% to 78% as τ decreases from 10^7 yr to 10^6 yr; the shorter migration timescale breeds fewer close encounters and fewer objects are lost to the competing 2:1 resonance. For $\tau = 10^5$ yr, $f_{3:2} \approx 30\%$.
3. At least 1 Twotino candidate having a large eccentricity has been observed. This observation, interpreted within the confines of our migration model, implies that τ cannot be equal to or lower than 10^5 yr. This conclusion is subject to the caveat that the migration model does not fully account for the observations; e.g., the model fails to generate the large orbital inclinations that are observed throughout the Kuiper Belt.

4. We have simulated the instantaneous spatial distributions of Twotinos and Plutinos as predicted by the migration model. If $\tau = 10^7$ yr, Twotinos cluster at longitudes displaced $\pm 75^\circ$ away from Neptune’s longitude, where the upper sign corresponds to those objects librating with low amplitudes, $\Delta\Phi_{2:1} \lesssim 1$ rad, about $\langle\Phi_{2:1}\rangle \approx \pi/2$, and the lower sign corresponds to objects librating with similarly low amplitudes about $\langle\Phi_{2:1}\rangle \approx 3\pi/2$. Plutinos cluster at longitudes displaced $\pm 90^\circ$ away from Neptune’s longitude, and all librate about $\langle\Phi_{3:2}\rangle = \pi$. Longitude-to-longitude variations in the sky densities of Plutinos and Twotinos persist even for surveys that are not volume-limited in their ability to detect resonant objects of a given size. These variations sharpen as the limiting distance out to which resonant objects can be detected decreases.
5. Over the longitude interval 210° – 240° (-90° to -60° of Neptune’s longitude), the bias in finding Plutinos over Twotinos is minimized. If the population of one resonance is identical to the other in terms of number, sizes, albedos, and orbital inclinations, then the migration model for $\tau = 10^7$ yr predicts 0.4 to 1 times as many Twotinos to be found over this longitude interval than Plutinos, as the limiting distance out to which objects are detected increases from 40 AU to ∞ . If $\tau = 10^6$ yr, the bias over this special longitude range varies from 0.4 to 1.1. A similar interval exists between 0° and 40° ($+60^\circ$ – 100° of Neptune’s longitude) if $\tau = 10^7$ yr, but does not exist if $\tau = 10^6$ yr (see next point).
6. The 2:1 resonance fills asymmetrically in the migration model—more objects are captured into libration about $\langle\Phi_{2:1}\rangle \approx 3\pi/2$ than about $\langle\Phi_{2:1}\rangle \approx \pi/2$. The difference between populations is $\sim 10\%$ if $\tau = 10^7$ yr, and increases to $\sim 330\%$ if $\tau = 10^6$ yr. We reserve an analytic explanation for our numerical discovery to future study.³ The asymmetry in libration centers translates directly into an asymmetry in the instantaneous spatial distribution of Twotinos—more Twotinos are expected to be found at longitudes behind that of Neptune than in front of it. A differential measurement of the Twotino density ahead and behind of Neptune would powerfully constrain the migration history of that planet.
7. Measuring the relative populations of Plutinos to Twotinos is a model-dependent enterprise. Under the assumption that Twotinos and Plutinos share the same sizes, albedos, and orbital inclinations, we employ the results in this paper to crudely de-bias the current tally of ~ 43 observed Plutinos to ~ 5 observed Twotinos to estimate an

³We have performed additional numerical and analytic studies that demonstrate that this asymmetry can be understood purely within the restricted, circular, 3-body problem where the perturber’s orbit expands outward.

intrinsic population ratio of $F = 2.7\text{--}3.6$. The range in our estimate reflects an order-of-magnitude difference in the assumed τ , from 10^7 yr to 10^6 yr. We suspect that our estimate is an upper limit because Plutinos probably enjoy a greater frequency of astrometric recovery than Twotinos, and because orbit fitting algorithms employed by the Minor Planet Center, whose dataset we use, favor Plutino-like trajectories. Improved estimates for F can be obtained by coupling our calculation to KBO surveys having well-documented discovery statistics. While it tentatively appears that Plutinos might intrinsically outnumber Twotinos by a factor not exceeding ~ 3 , this conclusion can but does not necessarily imply that the surface density of the primordial planetesimal disk dropped dramatically with distance in the vicinity of ~ 42 AU.

This work was supported by a National Science Foundation Planetary Astronomy Grant AST-0205892, two Faculty Research Grants awarded by the University of California at Berkeley, and a UC Berkeley Letters & Science Undergraduate Research Travel Grant awarded to ABJ. We thank Marc Buie, Jim Elliot, Susan Kern, Renu Malhotra, Bob Millis, David Trilling, and Larry Wasserman for encouraging discussions, and an anonymous referee for providing a critical and insightful report.

REFERENCES

- Allen, R.L., Bernstein, G.M., & Malhotra, R. 2001, *ApJ*, 549, L241
- Bernstein, G., & Khushalani, B. 2000, *AJ*, 120, 3323
- Borderies, N., & Goldreich, P. 1984, *Celest. Mech.*, 32, 127
- Brown, M.E. 2001, *AJ*, 121, 2804
- Chiang, E.I., & Brown, M.E. 1999, *AJ*, 118, 1411
- Cohen, C., Hubbard, E., & Oesterwinter, C. 1973, Elements of the outer planets for one million years, U.S. Naval Observatory Nautical Almanac, 22, 1
- Duncan, M.J., Levison, H.F., & Budd, S.M. 1995, *AJ*, 110, 3073
- Duncan, M.J., Levison, H.F., & Lee, M.-H. 1998, *AJ*, 116, 2067
- Fernandez, J.A., & Ip, W. H. 1984, *Icarus*, 58, 109
- Friedland, L. 2001, *ApJ*, 547, L75
- Gladman, B., et al. 1998, *AJ*, 116, 2042
- Henrard, J., & Lemaître, A. 1983, *Celest. Mech.*, 30, 197

- Ida, S., Bryden, G., Lin, D.N.C., & Tanaka, H. 2000, *ApJ*, 534,428
- Jewitt, D., Luu, J., & Trujillo, C. 1998, *AJ*, 115, 2125
- Jewitt, D.C., & Luu, J.X. 2000, in *Protostars and Planets IV*, eds. V. Mannings, A.P. Boss, and S.S. Russell (Tucson: University of Arizona Press), 1201
- Levison, H. F., & Stern, S.A. 1995, *Icarus*, 116, 315
- Levison, H. F., & Stern, S.A. 2001, *AJ*, 121, 1730
- Malhotra, R. 1995, *AJ*, 110, 420
- Malhotra, R. 1996, *AJ*, 111, 504
- Malhotra, R., & Williams, J.G. 1997, in *Pluto and Charon*, eds. S.A. Stern & D.J. Tholen (Tucson: University of Arizona Press), 127
- Malhotra, R., Duncan, M.J., & Levison, H.F. 2000, in *Protostars and Planets IV*, eds. V. Mannings, A.P. Boss, and S.S. Russell (Tucson: University of Arizona Press), 1231
- Millis, R., et al. 2002, *AJ*, 123, 2083
- Morbidelli, A., Thomas, F., & Moons, M. 1995, *Icarus*, 118, 322
- Morbidelli, A. 1997, *Icarus*, 127, 1
- Nesvorny, D., Roig, F., & Ferraz-Mello, S. 2000, *AJ*, 119, 953
- Peale, S.J. 1986, in *Satellites*, eds. J.A. Burns & M.S. Matthews (Tucson: Univ. Arizona Press), 159
- Wisdom, J., & Holman, M. 1991, *AJ*, 102, 1528
- Yu, Q., & Tremaine, S. 2001, *AJ*, 121, 1736

Table 1. Summary of Simulations

Label	$\tau(\text{yr})$	Resonance	$f(\%)^a$	$g(\%)^b$	$\langle\Phi\rangle \approx \pi (\%)^c$	$\langle\Phi\rangle \approx 3\pi/2 (\%)^c$	$\langle\Phi\rangle \approx \pi/2 (\%)^c$	Figures
Ia	10^7	3:2	23	46	100	0	0	3,5,6,10–12,14,16,17
Ib	10^7	2:1	53	50	16	44	40	4,5,7–11,13,15–17
IIa	10^6	3:2	78	92	100	0	0	6,20,21
IIb	10^6	2:1	15	50	13	67	20	18,19–21
IIIa	10^5	3:2	30	97	100	0	0	6
IIIb	10^5	2:1	0

^aEfficiency of capture into a given resonance.

^bEfficiency of retainment of captured objects by a given resonance over the age of the solar system. For the 2:1 resonance, this is assumed to be 50% (Malhotra 2002, personal communication). For the 3:2 resonance, we take the retained population to comprise those captured objects that either have $\Delta\Phi_{3:2} < 110^\circ$ or that inhabit Kozai-type resonances for which $\langle\omega\rangle = \pm 90^\circ$ (compare with Levison & Stern 1995).

^cPercentage of objects in the resonance that librate approximately about the mean value indicated.